ANNUAL REVIEWS

Annual Review of Chemical and Biomolecular Engineering

Zeolitic Imidazolate Framework Membranes: Novel Synthesis Methods and Progress Toward Industrial Use

Dennis T. Lee,[1,*] Peter Corkery,[1,*] Sunghwan Park,[1,*] Hae-Kwon Jeong,[2] and Michael Tsapatsis[1,3]

[1]Department of Chemical and Biomolecular Engineering and Institute for NanoBioTechnology, Johns Hopkins University, Baltimore, Maryland, USA; email: tsapatsis@jhu.edu

[2]Artie McFerrin Department of Chemical Engineering and Department of Materials Science and Engineering, Texas A&M University, College Station, Texas, USA; email: hjeong7@tamu.edu

[3]Applied Physics Laboratory, Johns Hopkins University, Laurel, Maryland, USA

Annu. Rev. Chem. Biomol. Eng. 2022. 13:529–55

First published as a Review in Advance on April 13, 2022

The *Annual Review of Chemical and Biomolecular Engineering* is online at chembioeng.annualreviews.org

https://doi.org/10.1146/annurev-chembioeng-092320-120148

*These authors contributed equally to this article

Keywords

membrane, distillation, metal–organic framework, separation, hydrocarbons, gas

Abstract

In the last decade, zeolitic imidazolate frameworks (ZIFs) have been studied extensively for their potential as selective separation membranes. In this review, we highlight unique structural properties of ZIFs that allow them to achieve certain important separations, like that of propylene from propane, and summarize the state of the art in ZIF thin-film deposition on porous substrates and their modification by postsynthesis treatments. We also review the reported membrane performance for representative membrane synthesis approaches and attempt to rank the synthesis methods with respect to potential for scalability. To compare the dependence of membrane performance on membrane synthesis methods and operating conditions, we map out fluxes and separation factors of selected ZIF-8 membranes for propylene/propane separation. Finally, we provide future directions considering the importance of further improvements in scalability, cost effectiveness, and stable performance under industrially relevant conditions.

1. INTRODUCTION

MOF: metal–organic framework

ZIF: zeolitic imidazolate framework

HmIM: 2-methylimidazole

Metal–organic framework (MOF) membranes are an emerging class of separation agents that hold promise for demanding separations in which other membrane types, such as polymer, facilitated transport, and carbon molecular sieve, have performance limitations (1–10). Zeolitic imidazolate frameworks (ZIFs), a subset of MOFs consisting of more than 200 characterized structures, have been studied for a range of applications, most notably for olefin/paraffin separations (11–21). Short-chain olefins—mainly ethylene, propylene, and butenes—are used as monomers in more than half of US plastics production, and separation from their (saturated) paraffin analogs is typically accomplished via distillation because it is a well-understood and reliable separation process that can achieve high product purity and recovery (12, 22, 23). However, distillation of these mixtures is energy intensive owing to the proximity of the species' relative volatilities, requiring columns that can contain 200 stages and operate at large reflux ratios, resulting in accordingly high capital and operating costs (22, 24–26).

Certain membrane-based separation processes can exploit differences in species' diffusivities to efficiently drive a separation and operate in a single phase under a pressure gradient. It has been argued that given their lower energy requirements, hybrid membrane/distillation systems using high-performance MOF, carbon molecular sieve, or facilitated transport membranes could lower the energy used for olefin/paraffin separation (12, 27).

ZIF-8, consisting of Zn centers bridged by 2-methylimidazole (HmIM) ligands, as shown in **Figure 1**, has been targeted for propylene/propane separations owing to a propylene diffusivity that is more than 100 times greater than that of propane (19, 20, 28, 29). Despite ZIF-8's crystallographically measured pore aperture size of 3.4 Å, the rotation of HmIM ligands allows molecules with kinetic diameters of up to 6.7 Å to diffuse throughout the framework (30, 31). However, a sharp drop-off in diffusivity for molecules with kinetic diameters of greater than 4.0 Å—considered the effective aperture size of ZIF-8—enables separation of propylene from propane (19, 29, 30).

In this review, we discuss important structural features of ZIF-8 and other ZIFs as they relate to their membrane performance. We also review many methods that can be used to make ZIF membranes and discuss issues regarding their scalability. In addition, we discuss permeation performance at conditions relevant to industrial use.

2. STRUCTURAL FEATURES OF ZIFS

ZIFs are made of divalent transition metal centers (mostly Zn^{2+} and Co^{2+}) tetrahedrally coordinated with imidazolate-based linkers (28, 32). Given the similarity in the M-Im-M bond angle of ZIFs to the Si-O-Si bond angle in zeolites, ZIFs tend to form in zeolitic topologies, hence the term zeolitic imidazolate frameworks. Through judicious choices of transition metal centers and imidazole linkers, ZIFs with diverse topologies have been synthesized (28, 32) (**Figure 1*a–c***). In this section, we present key structural and functional features of ZIFs, including framework flexibility and tunable properties enabled by choice of linkers and metals.

2.1. Framework Flexibility

The 6-membered ring window of ZIF-8 is responsible for its molecular sieving ability. The imidazole rings around the window define the aperture size. The imidazolate linker can swing relative to the 6-membered ring plane, effectively enlarging the aperture to ~4.0 Å (33, 34) (**Figure 1*d***). The flexibility of ZIF-8 is reflected on two distinct timescales: the above-mentioned dynamic vibration of the linker around its central position on the timescale of a picosecond and the guest-induced, quasi-static rotation of the equilibrium position itself.

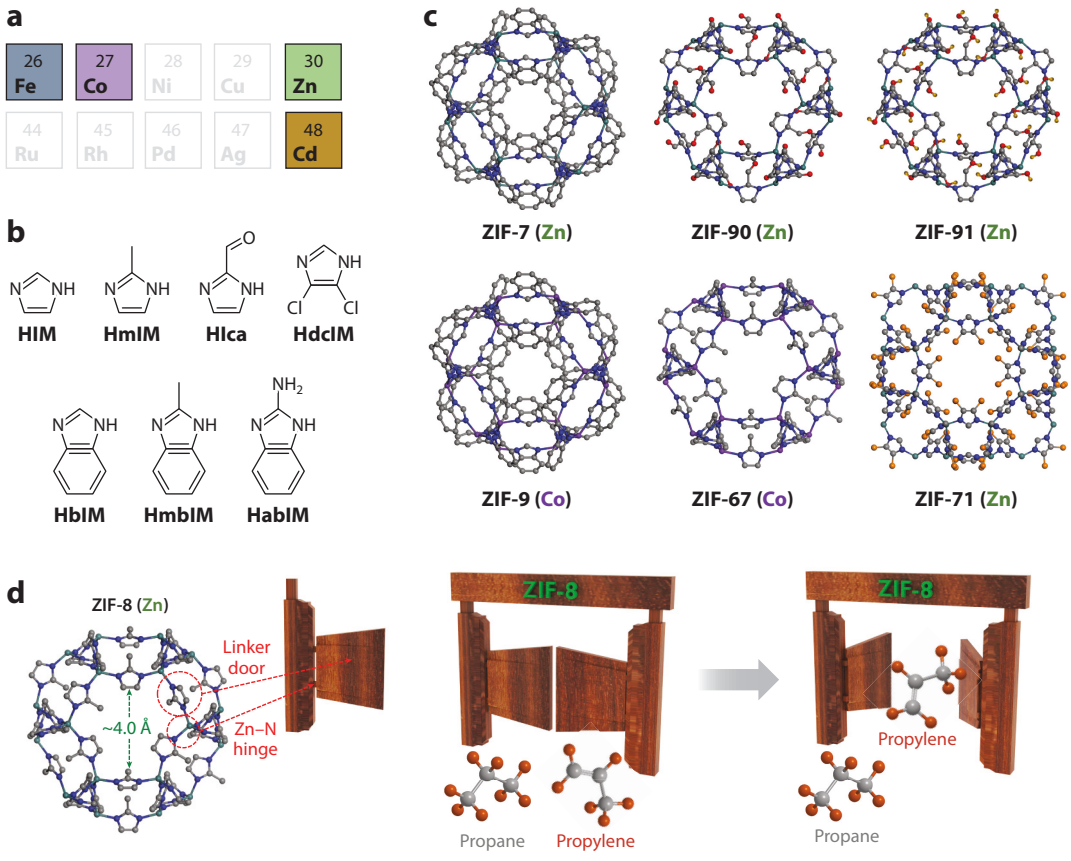

Figure 1

Selection of (*a*) metal elements and (*b*) organic linkers of ZIFs presented in this review. (*c*) Representative ZIF structures used for the powder synthesis and membrane fabrication for gas separation applications. (*d*, *left*) Flexibility of ZIF-8 structure with an effective aperture size of ~4.0 Å, larger than that (~3.4 Å) defined by crystallographic analysis. (*Right*) Schematic illustration of selective pass of propylene (~4.0 Å) over propane (~4.2 Å) by size through flexible ZIF-8. Abbreviations: HabIM, 2-aminobenzimidazole; HbIM, benzimidazole; HdcIM, 4,5-dichloroimidazole; HIca, imidazole-2-carboxaldehyde; HIM, imidazole; HmbIM, 2-methylbenzimidazole; HmIM, 2-methylimidazole; ZIF, zeolitic imidazolate framework.

Li et al. (20) first observed the remarkable difference between the adsorption kinetics of propane and propylene in ZIF-8 powders, despite the species having almost identical equilibrium isotherms and adsorption enthalpy. This discovery motivated simulations suggesting the imidazolate ring swings relative to the plane in an empty framework or an infinitely dilute adsorbate environment (33–35). The finite possibility of such swinging to the high angles (and thus larger aperture) accounts for the diffusion of large molecules through the aperture, which would be forbidden in a rigid framework model. The aperture can also be further braced open transiently to let larger molecules go through during intercage transport. The pore size and stiffness related to swinging are affected by the metal of the framework (36). Krokidas et al. (29) calculated the diffusivities of various gas molecules through ZIF-8 and ZIF-67 (i.e., ZIF-8 with cobalt centers). They found that the diffusivity behavior is correlated with the expansion ratio, i.e., the maximum aperture size in the intercage transition state versus penetrant molecular size. Note that the linker vibrates on a picosecond timescale or terahertz frequency (37) and thus is not probed directly by crystallography or equilibrium adsorption measurements.

HbIM: benzimidazole

PDMS: polydimethylsiloxane

When guest species are present in the framework, in addition to the vibrational swinging effect, the imidazolate linkers can rotate to new equilibrium positions with a nonzero torsion angle. The linker rotation is often accompanied by the expansion of the unit cell dimensions as the uptake increases. Depending on the context, such a transition is termed interchangeably as gate opening, ambient pressure/high pressure (34, 38–40), or low/high loading (41, 42). Likewise, the gate opening transition in ZIF-7 [a ZIF for which the HmIM linker of ZIF-8 is replaced by benzimidazole (HbIM)] is called narrow/large pore transition (11, 43, 44). Moggach et al. (38) first reported the structural change in ZIF-8 under 1.47 GPa hydrostatic pressure using a mixture of methanol/ethanol to compress ZIF-8 single crystals. At 1.47 GPa, the uptake of guest molecules in the framework increases significantly owing to the twisting of the imidazolate. Gate opening transition also results in a step in N_2 adsorption isotherm under 0.02 bar pressure (39) at 77 K and corresponds to a 26% N_2 uptake increase owing to the rearrangement of adsorbed molecules and the linker rotation, which opens up new adsorption sites near the 4-membered ring window.

Regarding diffusion, such gate opening can easily induce the high angle configuration, facilitating the passage of relatively large guest molecules (compared to the crystallographically determined pore openings) through the aperture. At high loading/pressure, the gate opening can be detrimental or beneficial to the selectivity for molecule pairs near the critical size of the aperture. As Du et al. (44) demonstrated via in situ X-ray diffraction experiments for ZIF-7 during alcohol adsorption, ethanol adsorption opens up the structure, compromising its ability for kinetic separation of 1-pentanol/ethanol. Another simulation study (45) suggests that the ZIF-8 unit cell keeps shrinking under pressures up to 1 GPa, and the aperture size is reduced by 0.3 Å at 1 GPa, leading to improved diffusion selectivity of propylene over propane, although the vibrational swinging amplitude remains the same (±1 Å).

The gate opening phenomenon is affected strongly by an interplay of guest species, pressure, and temperature. O_2 adsorption experiments (40) in ZIF-8 show that the gate opening effect is temperature dependent. In ZIF-7, the pressure of the gate opening transition was also found to increase at a higher temperature for CO_2 and CH_4 (43). Simulation results confirm that hydrocarbon adsorption does not promote the gate opening transition near room temperature (33), whereas the vibrational fluctuation amplitude of the aperture determining the maximum penetrable molecule size is temperature dependent (36).

ZIF-8 structural flexibility also depends on crystal size, adding to the complexity of its adsorption behavior. Zhang et al. (46) compared N_2 adsorption isotherms of bulk and nanosized ZIF-8. The transition pressure for gate opening increases significantly as the crystal size decreases owing to destabilized adsorption in the surface layer rather than structural differences. In contrast, Tanaka et al. (47) measured adsorption isotherms of Ar, N_2, and 1-butanol and concluded that the increased transition pressure for nanocrystals was due primarily to the suppressed framework flexibility of the outer layers. Tian et al. (48) observed, in addition to the upshifting transition pressure, a widening adsorption/desorption hysteresis loop in nanocrystals, suggesting a higher energy barrier for structural transition. A recent nanoindentation study (49) also found stiffness differences between nanosized ZIF-8 and microcrystals.

Sheng et al. (50) coated polycrystalline ZIF-8 membrane with polydimethylsiloxane (PDMS) and tested propylene/propane separation performance. They suggested that penetration of PDMS into the membrane blocks intercrystal defects and hinders the framework flexibility under high pressure so that the membrane selectivity of 100 is maintained at a cross-membrane pressure difference of 6 bar.

ZIF flexibility adds complexity and uncertainty when considered for practical membrane applications because, depending on membrane microstructure (e.g., grain size, porous support confinement, ZIF–support interface), feed and permeate composition, temperature, and pressure, the

effective pore openings can be altered from their nominal crystallographic values. This sensitivity to structure and operation conditions could also be viewed as an opportunity to optimize membrane performance.

SOD: sodalite

HIca: imidazole-2-carboxaldehyde

CdIF: cadmium imidazolate framework

2.2. Tunable Properties

ZIFs with a sodalite (SOD) topology, such as ZIF-7, ZIF-8, ZIF-9, ZIF-67, ZIF-90, ZIF-91, and ZIF-92, have been studied extensively for their gas separation applications owing to their relatively small effective aperture sizes (i.e., 3–5 Å), which make them suitable for the kinetic separation of relatively small penetrant gases and light hydrocarbons. Because the properties of SOD-ZIFs (also called ZIF-8 isostructures) depend on types of metal centers and linkers (51–53), we discuss how the properties of ZIF-8 isostructures—in particular, gas adsorption and diffusion—can be affected by different metal centers and/or linkers and can ultimately be tunable upon introduction of mixed metal centers and/or linkers.

2.2.1. Linker effects. Pore aperture size, framework flexibility, and affinity for adsorbate molecules in ZIF-8 isostructures (**Figure 1**) are strongly dependent on linkers. For example, the surface area of ZIF-90 (S_{BET} = 1,270 m^2/g) was reduced to S_{BET} = 1,010 m^2/g upon conversion to ZIF-91 with ∼80% reduction of the imidazole-2-carboxaldehyde (HIca) linkers to their alcohol derivative, whereas ZIF-92, containing ethanolamine groups in place of the carboxaldehyde groups of ZIF-90, displayed negligible N_2 adsorption, indicating that the bulkier linkers substantially reduced the aperture sizes (54). Both effective and nominal aperture sizes of ZIFs increase in the order of ZIF-7 < ZIF-8 < ZIF-90, although each structure shows different molecular sieving effects owing to the extent of attractive and repulsive forces between neighboring linkers (55, 56). For example, the gate opening of ZIF-90 occurred in a single step and at a higher relative pressure (i.e., P/P_0 = ∼0.4) than that of ZIF-8 (cf. the two-step gate openings of ZIF-8 at P/P_0 of ∼0.005 and ∼0.02, respectively) (54, 57), which was attributed to the reduced linker swinging owing to steric hindrance and different guest–host interactions (53, 58). Additionally, ZIF sorption capacity can be altered by chemical functionalization to improve guest–host interactions. CO_2 sorption capacity on ZIF-8, for example, can be increased by adding electron-donating amino groups ($–NH_2$) (59).

2.2.2. Metal center effects. Studies on the effects of metal centers have been less common owing to the poor stability of ZIFs containing metals other than Zn, Co, and Cd (32, 60, 61). However, the transition metal centers significantly affect the pore aperture size and linker swing motion. For the HmIM-based ZIFs with SOD topologies, the effective aperture sizes increase in the order of ZIF-67 (Co) < ZIF-8 (Zn) < CdIF-1 (Cd) (62–64), which is ascribed to the metal–linker bond length and stiffness (62). These factors contributed to the absence of distinct gate opening in the N_2 adsorption at 77 K for ZIF-67 and CdIF-1 (63, 65). For SOD ZIFs with HbIM linkers, the pressure-responsive phase transition behavior (i.e., pore breathing) of CdIF-13 (Cd) differed remarkably from that of ZIF-7 (Zn) and ZIF-9 (Co), likely owing to an increased flexibility with longer metal–linker bonds (66). Whereas a phase transition occurred at less than 1 bar for ZIF-7 (Zn) and ZIF-9 (Co) for CO_2 adsorption at ambient temperature, CdIF-13 (Cd) experienced a phase change at a significantly increased pressure of ∼11 bar and demonstrated a unique double-stepped pore-breathing phenomenon at higher temperatures (66).

2.2.3. Multicomponent effects. Hybrid ZIFs (also known as multicomponent ZIFs) contain multiple types of linkers and/or metals and can provide more systematic tunability of properties by controlling the composition ratios of linkers and/or metals (67, 68). Unlike the general

mixed-metal/linker ZIFs, which share a topology with parent ZIFs, metal/linker-doped ZIFs involve unsuitable secondary components, which alone cannot form the topologies of resulting multicomponent ZIFs (69, 70). Multicomponent ZIFs prepared via the in situ approach, in which both metal and linker species are present in the initial synthesis solution, have an even distribution of metal/linker components throughout the crystals and are referred to as homo-centered ZIFs. The postsynthetic approach involves placing as-formed single-component ZIFs in solutions containing either linkers or metals not present in the parent ZIFs (64). This process is referred to as solvent-assisted linker exchange (SALE) or postsynthetic ligand/metal exchange (71), which results in a core-shell structure in which the outer layers have had linkers or metals exchanged while the interior remained as the parent ZIF structure. In comparison to the single-component ZIFs (i.e., ZIF-8 and ZIF-90), ZIF-8–90 [$Zn(mIM)_x(Ica)_{2-x}$] prepared via the in situ approach exhibits gas adsorption and diffusion reflecting homogeneously changed pore characteristics (55, 57, 72). In contrast, the gas adsorption and diffusion properties of ZIF-8–90 prepared via the postsynthetic approach on ZIF-8 were comparable to those of a physical mixture of ZIF-8 and ZIF-90 owing to their segregated structure (i.e., ZIF-8-rich core and ZIF-90-rich shell) (72–74). These findings demonstrate that the spatial distribution of different linkers depends on the method used to synthesize the multicomponent ZIF, and frameworks with the same linker fractions could have different gas diffusivities (75, 76).

SALE: solvent-assisted linker exchange

DMF: dimethylformamide

3. ZIF SYNTHESIS

ZIF crystallization is usually performed in batch systems and follows typical nucleation and growth curves (77). To control the nucleation and the growth steps, diverse ZIF synthesis routes have been investigated (78–80). Solvent, metal/ligand precursor type and concentration, reaction conditions, and the presence of additives collectively determine ZIF properties such as shape, size, yield, purity, and crystallinity (81–84). Several ZIF preparation strategies, including solvo-/hydrothermal, ionothermal, mechanochemical, sonochemical, and microwave methods, have been inspired from similar approaches used successfully to make zeolites (85). Conventional solvo-/hydrothermal methods have been used most commonly for ZIF synthesis because they are convenient and high throughput and allow for precise control through the variation of synthesis parameters (e.g., temperature, time, solvent, precursor, modulator, and concentration) (32). In addition, electrochemical and vapor-phase methods that have not been applied to zeolite synthesis have been developed for ZIF synthesis. In the following discussion, we focus primarily on the synthesis of ZIF-8.

3.1. Conventional Solvothermal (Nonaqueous) Synthesis

Organic solvents, typically methanol or dimethylformamide (DMF), are commonly used for ZIF synthesis (28, 86). Although DMF serves as a structure-directing agent of ZIFs and provides relatively high yields (28, 78), alcohol-based synthesis can be performed at relatively mild temperatures and requires easier activation processes (removal of solvent from pores) than DMF-based synthesis (78, 87). In a methanolic ZIF-8 synthesis, Cravillon et al. (88) used in situ small- and wide-angle X-ray scattering to observe small clusters made of Zn^{2+} and HmIM in the early stages of the synthesis that later formed ZIF-8 particles, although the transition from cluster to nuclei is still not well understood. In a separate study using in situ light scattering for methanolic ZIF-8 synthesis, the same group observed that more basic modulating ligands increased the nucleation rate, resulting in a higher number of nuclei and a smaller average nucleus size than ZIF-8 synthesized using less basic modulating ligands (83).

In methanolic ZIF-8 synthesis, an increase in linker concentration was found to increase the number of nuclei and decrease the average nucleus size (89). This result was attributed to increased

deprotonation of HmIM groups bound to M^{2+} (Co or Zn) ions, allowing the HmIM ligands to bind to a neighboring metal ion to produce oligomers that can later form ZIF nuclei (89). Higher synthesis temperatures increased the average particle size while not affecting the particle density, indicating that temperature influences a crystal growth rate but has little effect on the nucleation rate (89).

3.2. Conventional Hydrothermal Synthesis

Aqueous ZIF synthesis is desirable for (*a*) environmental benefit, (*b*) mild and fast synthesis, and (*c*) high yield (90). It was first accomplished by the Lai group in 2011 (91). Jian et al. (82) performed a systematic investigation of the effect of important synthesis parameters and proposed a mechanism for ZIF-8 growth in a water-based system, consisting of (*a*) coordination, (*b*) deprotonation, and (*c*) ligand exchange (**Figure 2*a***). The first step is proposed to involve Zn ions coordinating with HmIM to form $Zn(HmIM)_n^{2+}$ ($1 \leq n \leq 4$, $pK_a = 10.3$) units. The bound HmIM groups in these $Zn(HmIM)_n^{2+}$ units must then be deprotonated before they can undergo ligand-exchange reactions to form larger species that will result in nuclei (83). The basic HmIM molecules ($pK_a = 14.2$) can remove a proton from a neighboring water molecule, forming H_2mIM^+ ($pK_a = 7.0$) molecules that can no longer coordinate to free Zn^{2+} atoms or deprotonate $Zn(HmIM)_n^{2+}$ units. Therefore, aqueous ZIF-8 synthesis requires a large excess of HmIM to form a basic solution in which there is a large concentration of the unprotonated HmIM, as shown in **Figure 2*b***.

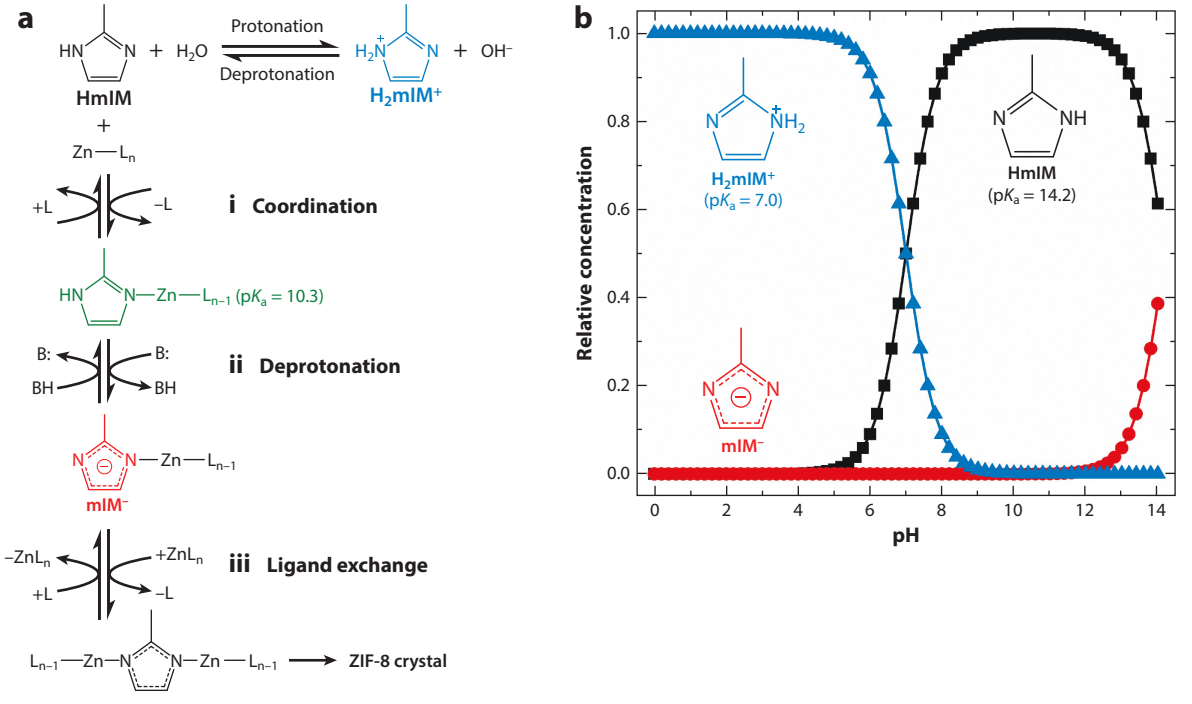

Figure 2

(*a*) Sequence of steps involved in the formation of ZIF-8 crystals in water. L indicates ligands that could be present, such as auxiliary modulating ligands, H_2O, NO_3^-, and MeOH. (*b*) Relative concentration of HmIM-based species (i.e., HmIM, H_2mIM^+, and mIM^-) as a function of pH in water in the absence of any other species. Abbreviations: H_2mIM^+, protonated 2-methylimidazolate; HmIM, 2-methylimidazole; mIM^-, deprotonated 2-methylimidazolate; ZIF, zeolitic imidazolate framework.

At relatively low linker-to-metal (L/M) ratios, zinc hydroxide and basic zinc nitrate are formed owing to insufficient deprotonation of HmIM (92–95). Pan et al. (91) reported the first synthesis of ZIF-8 in an aqueous solution, using an L/M ratio of 70. Diverse basic modulators have been employed for hydrothermal ZIF synthesis to enhance linker deprotonation (96–99), allowing phase-pure ZIF-8 to be synthesized at L/M ratios of 4:1 and 2:1 by using triethylamine (97) and ammonium hydroxide (98), respectively.

L/M: linker-to-metal

CVD: chemical vapor deposition

ZnO: zinc oxide

ALD: atomic layer deposition

MUV-3: Materials of University of Valencia

VPLE: vapor-phase linker exchange

3.3. Unconventional Solid- and Liquid-Phase Synthesis

Despite the simplicity and controllability of conventional solvo-/hydrothermal ZIF synthesis, the reaction provides low yields and is challenging to scale up (100). Additional external energies, such as mechanical force, ultrasound, microwave, and electric field, have been newly adopted for ZIF synthesis to overcome the limitations of conventional synthetic methods; these are well described in previous review papers (78, 80, 90, 100).

3.4. Vapor-Phase Synthesis

Vapor-phase ZIF synthesis is an emerging technique, providing unique features compared to liquid-phase counterparts.

3.4.1. Dry-gel conversion. The dry-gel conversion (steam-assisted conversion) method was one of the first attempts to avoid the use of organic solvents in synthesizing ZIFs. Shi et al. (101) reported that ZIF crystals were grown by water vapor–mediated reorganization of gel-phase eutectic mixtures of metal and ligand precursors. This synthesis technique offers shorter reaction times and high yields and minimizes, or completely avoids, the use of organic solvents (102). Whereas small amounts of vaporized water molecules were beneficial, excessive water generated undesirable dense phases (101). Chen et al. (103) used zeolites as a medium for solvent recovery to prevent the formation of undesirable impurities.

3.4.2. Chemical vapor deposition. Stassen et al. (104) introduced ZIF synthesis using chemical vapor deposition (CVD). They achieved the complete transformation of zinc oxide (ZnO) films less than 10 nm thick deposited by atomic layer deposition (ALD) to ZIF-8 via vapor–solid reaction of sublimated HmIM with the ZnO film (104). Owing to the different volumes per Zn atom within ZnO and ZIF-8, a substantial volume expansion has been observed upon conversion of ZnO to ZIF-8 (47, 104). Stassen and colleagues (105) also developed an integrated ALD–CVD process that produced ZIF films in a single reactor. Huang et al. (106) developed a direct synthesis approach called steam-assisted CVD using a flow-through reactor wherein Ar carrier gas was used to supply vapors of HmIM, cobalt acetylacetonate, and water to a sapphire substrate to grow thin films of ZIF-67. Steam-assisted CVD allowed for greater control over film orientation, grain size, and surface morphology than vapor-phase conversion of ZnO to ZIF (106). López-Cabrelles et al. (107) performed a direct vapor-phase synthesis of ZIF-8 by heating HmIM and a volatile Zn precursor under vacuum. They also synthesized Fe-ZIF-8 (referred to as MUV-3) using an analogous route (107).

3.4.3. Vapor-phase linker exchange. More recently, a postsynthetic ligand-exchange approach, wherein as-synthesized ZIFs in powder or film form are exposed to organic ligand vapors [i.e., vapor-phase linker exchange (VPLE)], has been developed as an alternative to SALE (108, 109). In contrast to the diffusion-limited SALE, vaporized linker diffusion through ZIF pores was not a rate-determining step, and there was no dissolution and recrystallization during the linker

exchange (108). The pore properties of ZIFs were effectively tuned via VPLE, while their original topologies were preserved (109, 110). In addition, the versatility of VPLE with diverse organic linkers was demonstrated, although an optimal combination of linker pK_a and vapor pressure is required to succeed in the exchange process (108, 110).

4. ZIF MEMBRANE FORMATION

A wide range of ZIF membranes, supported on porous ceramic or polymeric substrates with diverse geometries, have been reported and have shown potential for separating gas mixtures by molecular sieving or sorption selectivity (111, 112) (**Figure 3**, **Table 1**). To be exploited successfully in a membrane system, a supported ZIF layer must not only be well intergrown and defect free to minimize nonselective transport channels but also be very thin, desirably less than ~1 μm, to provide a high-throughput separation (113). Over the past decade, diverse and creative methods have been developed to fabricate high-performance ZIF membranes (114). In addition, postsynthetic treatments of as-formed ZIF membranes with organic linkers (109, 115), metal-containing precursors (116), or a short electron beam irradiation (117) have been developed recently to effectively modify ZIF membrane performance.

4.1. Support Effects

A range of innovative synthetic methods have been developed to improve the integration of ZIF layers into ceramic and polymeric supports for membrane preparation (**Figure 3** and **Table 1**).

4.1.1. Ceramic. Given their outstanding resistance to chemical, thermal, and mechanical stress, as well as their high porosity, porous ceramic supports, mostly made from Al_2O_3, TiO_2, SiO_2, or ZrO_2, have been used widely to form ZIF membranes (118). However, the thermal expansion coefficient mismatch between the ceramic support and the ZIF membrane layer could lead to substantial film cracking during the synthesis process, which limits the selection of membrane materials (119). The high manufacturing cost for ceramic supports compared to that of polymeric supports also restricts the use of ceramic ones to particular applications where polymeric components cannot be deployed (120).

In 2009, Bux et al. (31) showed promise with the first ZIF-based membrane for H_2/CH_4 separation by growing ZIF-8 directly on asymmetric TiO_2 (rutile and anatase compound) disks via a microwave-assisted solvothermal approach. Based on microwave dielectric heating (121) coupled with conventional heating (**Figure 3*b***), the synthesis process facilitated rapid growth (~4 h) of a dense polycrystalline ZIF layer on the porous support. Although direct growth of ZIFs on unmodified support is a relatively simple process, it induces poor film continuity and membrane-layer delamination, responsible for nonselectivity in gas separation performance (122) owing to the unfavorable ZIF nucleation on the chemically inert supports. This also leads to undesirable ZIF crystals homogeneously grown in a liquid phase, generating costly precursor wastage (111). Surface modification of the porous supports with covalent linkers can increase the density of heterogeneous nucleation sites for ZIFs and enhance the interfacial compatibility between the ZIF layers and the supports (113), improving membrane quality and reducing the use of precursors. For instance, α-Al_2O_3 and TiO_2 disks, functionalized with 3-aminopropyltriethoxysilane via an imine condensation reaction, enable robust adhesion of well-intergrown ZIFs including ZIF-8, ZIF-7, ZIF-22 (123), and ZIF-90 (124) to the modified supports. Seeding with ZIF crystals or reactive precursors (i.e., metal precursors or organic ligands) (125) has been employed as a facile in situ route to promote heterogeneous ZIF nucleation and growth, yielding continuous ZIF membranes. α-Al_2O_3 supports seeded with as-synthesized ZIF crystals by an in situ

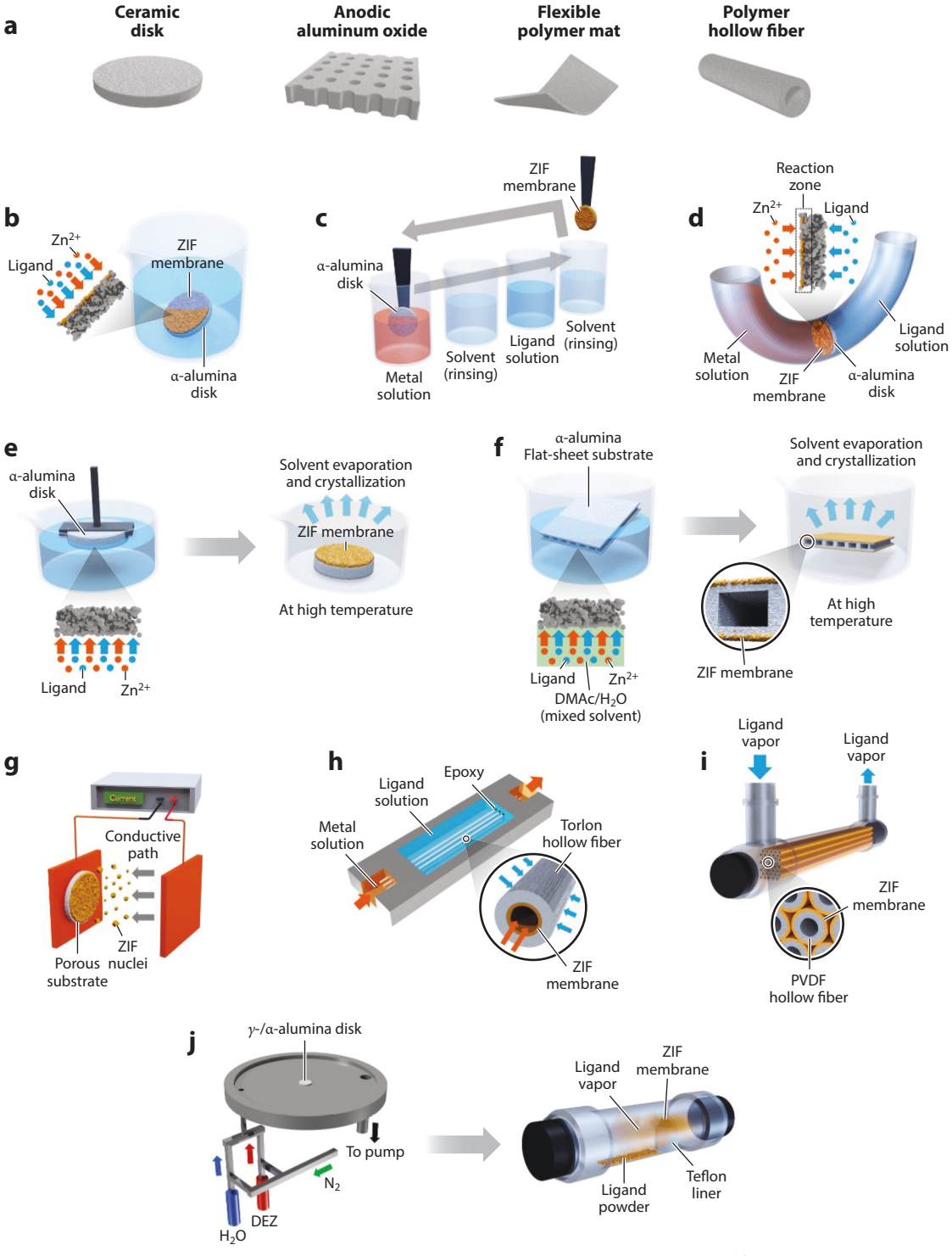

(*Caption appears on following page*)

Figure 3 (*Figure appears on preceding page*)

(*a*) Type of supports that have been used for ZIF synthesis. Schematic of representative ZIF membrane synthesis methods: (*b*) Solvo-/hydrothermal; (*c*) liquid-phase epitaxy; (*d*) counterdiffusion; (*e*) rapid thermal deposition; (*f*) dip coating-thermal conversion; (*g*) electrochemical deposition; (*h*) interfacial microfluidic membrane processing; (*i*) gel-vapor deposition; and (*j*) ligand-induced permselectivation. Abbreviations: DEZ, diethylzinc; DMAc, dimethylacetamide; PVDF, polyvinylidene fluoride; ZIF, zeolitic imidazolate framework.

microwave-assisted method (126, 127) or by simple slip-coating (6) have successfully reduced homogeneous nucleation and promoted the growth of thin and crack-free ZIF layers that are strongly adhered to the support. Kwon et al. (9) fabricated the first high-quality ZIF-67 membranes with sub-1-μm thickness through the heteroepitaxial solvothermal growth of ZIF-67 on ZIF-8 seed layers predeposited on α-Al_2O_3 disks via rapid microwave-assisted seeding. It was substantiated that dense ZIF-8 seed components, firmly anchored to the supports, enable the formation of a well-intergrown ZIF-67 layer; without the seeds, a defective ZIF-67 layer is formed.

The liquid-phase epitaxy approach, adopted by Shekhah et al. (128), enables the growth of a continuous and relatively thin (less than 1.5 μm) ZIF-8 layer on porous α-Al_2O_3 supports at room temperature, with the film thickness controlled simply by the number of the liquid-phase epitaxy cycles (**Figure 3*c***). This room-temperature technique prevents crack formation in the ZIF-8 film, which generally occurs upon heating–cooling processes in the conventional synthesis method owing to the difference in thermal expansion coefficients between the support and the film. However, there are certain drawbacks, such as the long processing time and the solution contamination as the deposition cycle is repeated.

The counterdiffusion (CD) concept as a sole method allows multiple uses of the expensive precursor solutions for synthesizing well-intergrown ZIF membranes with excellent microstructure or healing as-formed membranes with poor film continuity (129) (**Figure 3*d***). Xie et al. (130) created a continuous ZIF-8 membrane by adopting a new strategy, in which chemically modified α-Al_2O_3 particles are densely deposited onto a macroporous α-Al_2O_3 tube (average pore size of 3 μm), followed by a CD membrane synthesis in liquid phase at elevated temperature.

The membrane synthesis mechanism for the rapid thermal deposition (RTD) (131) (**Figure 3*e***) and the dip coating–thermal conversion (DCTC) (132) (**Figure 3*f***) methods is based on evaporation-induced crystallization (133), wherein the flow of the precursor solution is driven from inside the porous support to outside at an elevated temperature, which induces well-intergrown ZIF-8 membrane in less than 15 min. This rapid synthesis protocol offers excellent potential, including reducing cost and waste and enhancing scalability.

Ma et al. (12) fabricated the ultrathin ZIF-8 nanocomposite membranes by using an all-vapor-phase processing method, called ligand-induced permselectivation (LIPS), wherein the ALD-deposited ZnO layer transforms into the ZIF-8 layer by employing the ligand-vapor treatment (**Figure 3*j***). The distinct feature of the ZIF-8 layer made in this approach, compared to those prepared by other synthesis techniques, is that the selective layer is physically confined within the top 200 nm of the mesoporous (2–5-nm) γ-Al_2O_3 layer coated on the base α-Al_2O_3 support. This solvent- and seed-free approach performed in the all-vapor-phase shows promise in scalability.

In addition to an archetypical ZIF-8, Hao et al. (134) prepared continuously intergrown ZIF-67 and ZIF-90 membranes at sub-1-μm thickness in 8 min at room temperature via a CUSP (crystallization using sustained precursors) route (**Table 1**). As two peristaltic pumps continuously supply each precursor solution into a mixing chamber containing anodized aluminum oxide (AAO) substrates seeded with ZIF nuclei, a high growth rate is maintained while precluding Ostwald ripening, which typically occurs in conventional batch reaction systems. The same group also reported the rapid deposition of continuous and ultrathin ZIF films (i.e., ZIF-7 and ZIF-8) on various untreated substrates using a novel and potentially scalable electrophoretic nuclei assembly

CD: counterdiffusion

RTD: rapid thermal deposition

DCTC: dip coating–thermal conversion

LIPS: ligand-induced permselectivation

AAO: anodized aluminum oxide

Table 1 Aspects of representative synthesis methods for ZIF membrane synthesis with an assessment of membrane quality and scalability

Method	Support	Geometry	No. of steps	Condition		Membrane thickness	Specific requirement	Scalability rating	Synthesis methods (panel in Figure 3)	Reference(s)
				Temperature	Time					
In situ growth	Polymer, ceramic	Flat, tubular, HF	1	<100°C	>4 h	~40 μm	-	★☆☆☆	*b*	31
Seed-secondary growth	Polymer, ceramic	Flat, tubular, HF	2	<100°C	<6 h	~1 μm	-	★★★★	*b*	126, 127
RTD (rapid thermal deposition)	Ceramic	Flat	2	200°C	<15 min	<20 μm	-	★★★☆	*e*	131
DCTC (dip coating–thermal conversion)	Ceramic	Flat	2	200°C	<15 min	~560 nm	-	★★★★	*f*	132
LPE (liquid-phase epitaxy)	Ceramic	Flat	>10	RT	>8 h	<1.5 μm	-	★☆☆☆	*c*	128
CD (counterdiffusion)	Polymer, ceramic	Flat	1	RT	<72 h	16 μm	-	★☆☆☆	*d*	142
	Ceramic	HF	2	120°C	~5 h	<1 μm	-	★★☆☆	*d*	129
CUSP (crystallization using sustained precursors)	Ceramic	Flat	1	RT	<20 min	<1 μm	-	★★☆☆	*b*	134
ENACT (electrophoretic nuclei assembly for crystallization of highly intergrown thin films)	Polymer, ceramic	Flat	2	RT	>10 h	<3 μm	ED	★☆☆☆	*g*	135
FCDS (fast current-driven synthesis)	Ceramic	Flat	1	RT	<20 min	~200 nm	ED	★☆☆☆	*g*	136
ACD (aqueously cathodic deposition)	Ceramic	Flat	1	RT	<60 min	<500 nm	ED	★☆☆☆	*g*	137
IMMP (interfacial microfluidic membrane processing)	Polymer	HF	1	<42°C	>6 h	~10 μm	-	★★★☆	*b*	7, 157
GVD (gel-vapor deposition)	Polymer	HF	2	150°C	<6 h	~17 μm	-	★★★★	*i*	150
LIPS (ligand-induced permselectivation)	Polymer, ceramic	Flat, tubular, HF	2	>125°C	>24 h	<1 μm	Atomic layer deposition	★★☆☆	*j*	12
PMMOF (polymer modification–enabled in situ metal–organic framework formation)	Polymer	Flat, HF	3	120°C	~3 h	<1 μm	Polyimide	★★☆☆	*b*	179
Melt extrusion	Ceramic	Flat	2	440°C	>48 h	>20 μm	Metal–organic framework glass	★★★☆	*b*	180

Abbreviations: HF, hollow-fiber; RT, room temperature; ZIF, zeolitic imidazolate framework.

for crystallization of highly intergrown thin films (ENACT) approach (135) (**Figure 3*g***). In this process, the electric field induces the assembly and transfer of the charged ZIF nuclei toward the nonconductive AAO support positioned on the cathode, leading to the formation of highly permselective ZIF-based membranes. Similar methods with slight modifications, such as a fast current-driven synthesis (136) and an aqueously cathodic deposition (137), have been developed recently to synthesize bimetallic $Zn_{(100-x)}Co_x$-ZIF and ZIF-8 membranes, respectively, with improved propylene/propane separation performance (138).

ENACT: electrophoretic nuclei assembly for crystallization of highly intergrown thin films

HF: hollow fiber

PSF: polysulfone

PAN: polyacrylonitrile

4.1.2. Polymeric. Using polymeric rather than ceramic materials for making supports has advantages, including high processability, lower costs, and lower energy consumption (139). Supports with a hollow-fiber (HF) geometry, for example, can be assembled into compact modules with large membrane surface areas suitable for industrial gas separation applications (140). The main challenge with polymeric substrates, however, is that they easily experience uneven swelling during liquid-phase chemical modification or ZIF integration into the substrates, deteriorating the continuity of ZIF layers on polymeric supports (141).

Not until Yao et al. (142) demonstrated ZIF-8 membrane growth on flexible fibrous nylon membrane supports in 2011 did porous polymer-supported ZIF membranes emerge. The cyclic CD method (**Figure 3*d***) performed at room temperature keeps the polymeric support stable during synthesis, leading to a continuous and dense but quite thick (~16-μm) ZIF-8 layer. The conventional solvothermal seeded approach has also been applied directly to asymmetric polysulfone (PSF) porous sheets for the in situ integration of ZIF-8 membranes (143). Given its good chemical resistance and high service temperature (~150°C), the flexible PSF support acts as a stable platform on which a compact and intergrown ZIF-8 layer is grown in a methanolic solution at 90°C. Owing to precursor infiltration deep into the porous substrate, the ZIF-8 layer adheres strongly to the support but has a thickness of ~35 μm.

To promote stable ZIF layer integration, chemical modification of polymer supports must be tailored to the reactive groups present within the polymer. Polyacrylonitrile (PAN) possesses ample nitrile groups (–CN) that can be hydrolyzed into carboxylic acid groups (–COOH) in the presence of NaOH (144), whereas primary amines can ammoniate nonpolar polyvinylidene fluoride to generate amino groups ($–NH_2$) (145). The produced chemical functional groups provide a polymer surface with dense and adhesive heterogeneous nucleation sites for ZIF growth. As an added benefit, the polymer macromolecules crosslinked during the synthesis reduce the swelling and flexibility of the polymeric substrate, preventing substantial structural distortion in the ZIF layer under hydrostatic compression. A vapor-phase chemical modification with ethylenediamine at room temperature has been implemented for an asymmetric bromomethylated poly(2,6-dimethyl-1,4-phenylene oxide) support, giving rise to not only a reduction in substrate pore size but also a high density of nucleation sites, both of which are necessary for the formation of a thin and pinhole-free ZIF layer (146, 147). Neelakanda et al. (122) sputtered ~90 nm of ZnO film onto PAN porous supports, followed by dipping the samples into aqueous precursor solution at room temperature to synthesize ZIF-8 membranes. The precoated ZnO components function as nucleation sites and a metal source to realize continuous and thin ZIF-8 films with reduced penetration into the supports. Surface pretreatment is no longer necessary, however, if the pure polymeric component interacts strongly with precursors for membrane growth. A poly-thiosemicarbazide, which has an innate ability to chelate or bind a wide range of metals, is an excellent example of support with no need for surface pretreatments. Barankova et al. (148) demonstrated that a highly dense, crack-free, and thin ZIF-8 layer can be integrated directly onto the bare porous poly-thiosemicarbazide support via a simple CD synthesis.

IMMP: interfacial microfluidic membrane processing

GVD: gel-vapor deposition

C_3H_6: propylene

Macroporous HFs, consisting of chemically and mechanically resistant poly(amide-imide) Torlon®, prepared by a fiber-spinning process, have been successfully coated with molecular sieving layers of ZIF-8 (7) using seeded growth and interfacial microfluidic membrane processing (IMMP) (**Figure 3*b***). By dissolving the metal precursor and linker in separate immiscible solvents and maintaining the interface between the solvents on the inner surface of the fiber, IMMP enables the formation of thin defect-free ZIF membranes with correspondingly high permeance and selectivity. Potentially, this approach can position the ZIF layer even at the outer surface or in the bulk of the fiber by controlling the precursor and solvent locations, which influences the membrane performance. Su et al. (149) first introduced metal-based gels deposited on the polymeric HF support to synthesize continuous and stiff ZIF/polymer composite membranes. The Zn-based gel, impregnated in the porous substrate, transforms into ZIF during solvothermal treatment, ensuring robust adhesion between the ZIF layer (~20 μm) and the support. Li et al. (150) demonstrated the Zn-based gel transformation into ZIFs under a solvent-free environment using a gel-vapor deposition (GVD) method (**Figure 3*i***), leading to a significant reduction in ZIF layer thickness down to less than 20 nm. The versatile method also works well with a range of polymeric substrates, such as PAN, polyvinylidene fluoride, PSF, and polyethersulfone HFs, exhibiting an excellent gas separation performance.

4.2. Synthesis–Microstructure–Performance Relationship

In the traditional in situ solvothermal approach, in which ZIF association and dissociation occur simultaneously, it is challenging to control microstructural components of the selective layer, such as thickness, orientation, grain boundary defects, and rigidity (112, 114). Controlling these microstructures is critical, however, as it dictates membrane performance. Solution-based membrane synthesis methods relying on support modification (151), seeded growth (2, 6, 126, 152), and CD (129, 153–156) have improved membrane continuity while simultaneously limiting membrane thickness, thus enhancing membrane performance relative to in situ methods (**Figure 3** and **Table 1**). Some membranes relying on modified forms of ZIF-8, such as confined solvent molecules (132), ZIF-67 layers heteroepitaxially grown from ZIF-8 seed layers (9), and a stiffer ZIF-8 phase (136), have achieved much higher selectivities than standard ZIF-8 membranes and are discussed in greater detail in Section 5 (**Figure 3** and **Table 1**). Vapor-phase syntheses have been developed wherein permselective ZIF layers have been formed via conversion of impermeable layers consisting of Zn-based gels (150) or ALD ZnO deposits (12) to produce very thin membranes with minimal defects that display accordingly high selectivities and fluxes (**Figure 3** and **Table 1**). Membranes with selective layers confined within the support (12, 157) or coated with PDMS (50, 158) have maintained stable performance at elevated feed pressures, whereas membranes with selective ZIF layers grown out of the porous support (not confined) have typically performed poorly at these operating conditions, as is discussed in depth in Section 5 (**Figure 4**).

5. C3 SEPARATION BY ZIF MEMBRANES

5.1. C3 Separation by Membranes

Propylene (C_3H_6) is an important building block for many chemicals, including polypropylene; with an annual production of approximately 108 million metric tons in 2020, it is the second largest chemical commodity, following ethylene (159). Currently, most propylene is produced by steam cracking of naphtha and catalytic cracking of gas oils, both of which produce several chemicals, including ethylene, and subsequently require a series of separations, including ethylene/ethane and propylene/propane separations. Propylene and propane are separated in fractional distillation columns (called C3 splitter). Owing to their close boiling points, the C3 splitter requires a large

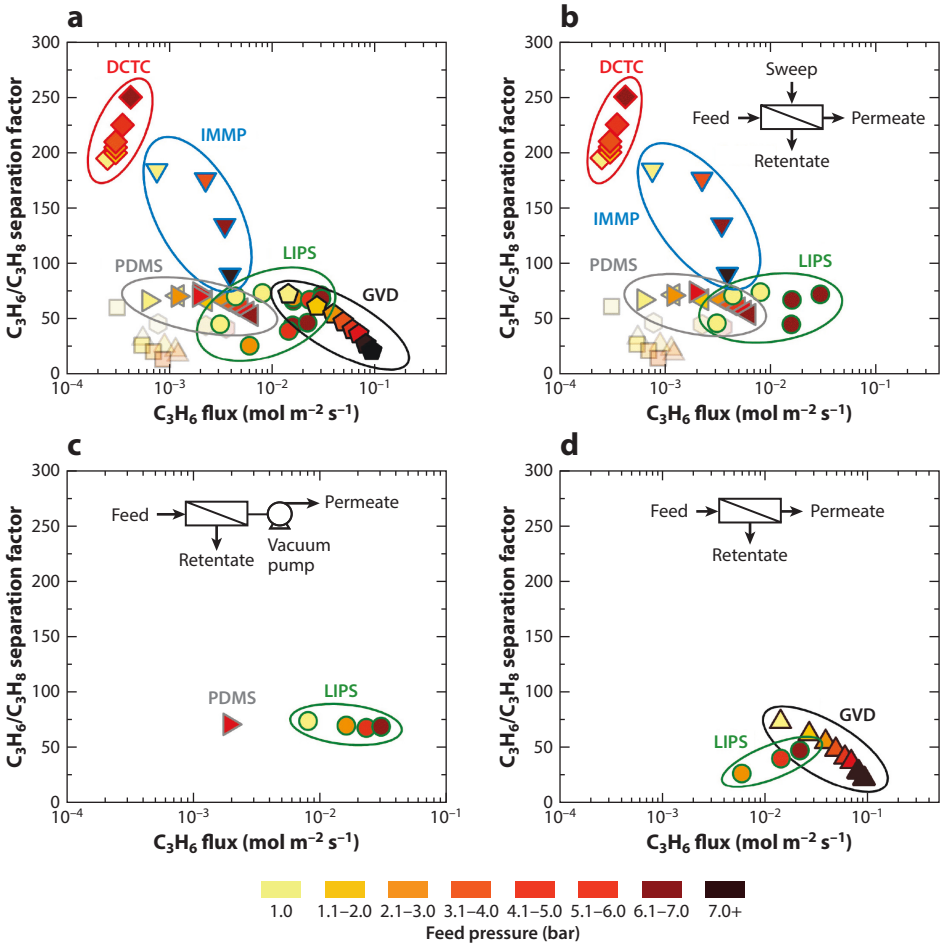

Figure 4

Representative ZIF-8 membrane performance including elevated feed pressure (1–9 bar). (*a*) Aggregate data. (*b*) Data collected using a sweep gas on permeate side. (*c*) Data collected using vacuum on permeate side. (*d*) Measurements obtained with 1 bar undiluted permeate. PDMS refers to ZIF membranes coated with a PDMS layer. All other initials correspond to the synthesis methods depicted in **Figure 3** [PDMS coating (*left-pointing triangle*, 50; *right-pointing triangle*, 158); seed solution dip-coating (*up-pointing triangle*, 2); IMMP (*down-pointing triangle*, 157); DCTC (*diamond*, 132); ZnO seed layer sputter-coating (*square*, 168); in situ ligand doping (*hexagon*, 178); GVD (*pentagon*, 150); LIPS (*circle*, 12)]. Abbreviations: DCTC, dip coating–thermal conversion; GVD, gel-vapor deposition; IMMP, interfacial microfluidic membrane processing; LIPS, ligand-induced permselectivation; PDMS, polydimethylsiloxane; ZIF, zeolitic imidazolate framework; ZnO, zinc oxide.

number of trays (150–250) with a high reflux ratio (15–25), resulting in high capital investment and energy costs (1, 160). Membrane-based C3 separation has been studied extensively as a cost-effective and energy-efficient alternative to the conventional distillation process.

5.2. C3-Selective ZIF-8 Membranes

Li et al. (20) reported a pioneering work on the kinetic uptakes of propylene and propane in ZIF-8 and its derivates and showed that propylene diffuses two orders of magnitude faster than propane.

Molecular sizes of C_3H_6 and propane (C_3H_8) are ~4.0 Å and ~4.2 Å, respectively. Though the crystallographically defined aperture size of 6-membered rings in ZIF-8 is 3.4 Å, the swing motion of the linkers makes its effective aperture substantially larger (**Figure 1*d***). Zhang et al. (161) estimated the effective aperture at 4.0–4.2 Å based on experimental observations.

C_3H_8: propane

GPU: gas permeance unit; 100 GPU = 3.35×10^{-8} mol/m^2 s Pa

Cm: monoclinic crystal system

I-43m: cubic crystal system

DZIF-8: defective ZIF-8

In 2012, Lai and his coworkers (6) reported the first propylene-selective ZIF-8 membranes. The membranes showed an average propylene permeance and C3 separation factor of ~50 GPU (100 GPU = 3.35×10^{-8} mol/m^2 s Pa) and ~35, respectively. Shortly after, Jeong's group (126, 129, 131, 153) reported a series of propylene-selective ZIF-8 membranes with an average propylene permeance of ~90 GPU and a C3 separation factor of ~50, respectively. Later, the same group demonstrated that ZIF-67 membranes showed a much enhanced C3 separation factor of ~209 with propylene permeance of ~50 GPU (9). The increased C3 separation factor of ZIF-67 membranes was attributed to the tempered linker rotation resulting from stiffer Co-N bonds. In 2018, Zhou et al. (136) reported a fast current-driven synthesis strategy to prepare ZIF-8 membranes with ultrahigh propylene selectivities. They found that under fast current, ZIF-8 crystalizes in a monoclinic (Cm) system rather than in a typical cubic (I-43m) system. The linkers in ZIF-8_Cm are less likely to rotate than those in ZIF-8_I-43m, thereby showing a significant increase in the propylene/propane separation factor of ~300 with a propylene permeance of ~50 GPU.

To process a large volume of gases, it is highly desirable to have membranes of high propylene permeance. As such, there is great interest in preparing membranes that are as thin as possible. For reference, commercial polymer membranes have thin selective skin layers of less than 200 nm. For polycrystalline membranes, whether zeolite or MOF membranes, thickness is determined by the chemistry of materials, the physicochemical properties of supports, and the processing methods. To prepare ultrathin (i.e., sub-500-nm) ZIF membranes, researchers have used supports with smooth surfaces, such as AAO. For example, He et al. (135) prepared ultrathin ZIF-8 membranes on AAO disks using the ENACT method. The resulting membranes were ~500 nm thick and showed a C_3H_6 permeance of ~300 GPU with a C_3H_6/C_3H_8 separation factor of 32. Wei et al. (137) prepared ZIF-8 membranes on AAO disks using the cathodic deposition method. The membranes showed a C_3H_6 permeance of ~180 GPU and a C_3H_6/C_3H_8 separation factor of ~140.

Recently, vapor-phase synthesis of ZIF membranes has gained significant research interest. Note that vapor-phase synthesis used for ZIF membranes so far is, strictly speaking, vapor-phase transformation of ZnO films to ZIF membranes. Tsapatsis's group (12) reported vapor-phase synthesis of ultrathin amorphous ZIF membranes supported on γ-Al_2O_3-coated α-Al_2O_3 substrates that displayed a propylene permeance of ~480 GPU and a propylene/propane separation factor of ~75 with stable on-stream performance over 10 days up to the feed pressure of 7 atm. Li et al. (150) prepared ZIF-8 membranes using gel-vapor transformation with a C_3H_6 permeance of ~830 GPU and a C_3H_6/C_3H_8 separation factor of ~70 owing to their thin selective layers of ~87 nm. Most recently, Qiao et al. (162) presented one of the thinnest ZIF-8 membranes supported on commercial ultrafiltration PSF filters, using interface layer polarization induction. The resulting defective ZIF-8 (DZIF-8) membranes were 45 nm thick and showed a record-high propylene permeance of ~3,000 GPU and a propylene/propane separation factor of ~90. The high C3 separation factor of the DZIF-8 membranes was attributed to abundant open metal sites capable of forming π bond interactions with propylene molecules.

Lee et al. (115) prepared highly permeable ZIF-8 membranes with an effective thickness of 250 nm using a SALE strategy. ZIF-8 linkers (HmIM) of micron-thick ZIF-8 membranes were partially exchanged with ZIF-90 linkers (HIca). Because ZIF-90 has a greater effective aperture than ZIF-8, the resulting ZIF-90/-8 hybrid membranes showed a fourfold increase in propylene

permeance (~230 GPU) while preserving the propylene/propane separation factor (~40). Based on increased propylene permeance, the effective thickness of the ZIF-8 layer was estimated at ~0.25 μm.

It is critically important to use scalable supports for ZIF membranes. Ceramic HFs and tubes as well as polymer HFs are more scalable than planar supports. Huang et al. (163) reported ZIF-8 membranes on yttria-stabilized zirconia HFs, achieving a propylene/propane separation factor of ~140 with a relatively low propylene permeance of ~16 GPU. Lee et al. (164) prepared ZIF-8 membranes on Al_2O_3 tubes using microwave-assisted seeding and secondary growth. The membranes showed a propylene permeance of ~50 GPU and a propylene/propane separation factor of ~200.

Compared to ceramic HFs/tubes, polymer HFs are more attractive as low-cost scalable supports. Eum et al. (157) were the first to report highly propylene-selective ZIF-8 membranes supported on poly(amide-imide) HFs (Torlon) using the IMMP method. The membranes exhibited a propylene permeance of ~45 GPU and a propylene/propane separation factor of ~180 at 1 bar and 25°C. The membranes showed stable performances even after continuous operation over 30 days. Lee et al. (165) reported sub-1-μm-thick ZIF-8 membranes on Matrimid® 5218 HFs showing a propylene permeance of ~5 GPU and a propylene/propane separation factor of ~46. Recently, Rashidi et al. (166) reported polycrystalline Mobil-type five (MFI)-type zeolite/ZIF-8 hybrid membranes on polymer HFs. Owing to the presence of more permeable MFI, the hybrid membranes exhibited a high propylene permeance of ~61 GPU with a propylene/propane separation factor of ~150.

The majority of ZIF-8 membrane articles have used mixed propylene/propane feed streams at atmospheric pressure (1 bar) with sweep gas on the permeate side, whereas commercial C_3H_6/C_3H_8 gas separation will require feed pressures of up to 15 bar and will not use a sweep gas (167). As shown in **Figure 4**, methods that localize the selective ZIF layer within the support (12, 157), as opposed to on the support surface, or that coat the membrane surface with PDMS (50, 132, 158) maintained high selectivities at high pressure, possibly owing to enhanced rigidity from the confinement of the ZIF structures. In contrast, some supported ZIF membranes showed a sharp decline in selectivity at increased pressures owing to increased propane permeance (150, 168). Ma et al. (132) prepared ZIF-8 membranes using a DCTC method that demonstrated an ~25% increase in selectivity as feed pressure was increased from 1 to 7 bar owing to dimethylacetamide molecules confined within the pores of the ZIF. As shown in **Figure 4*d***, membrane separation factors are much lower in mixed-gas testing with permeate that does not use sweep (**Figure 4*b***) and is not under vacuum (**Figure 4*c***). As feed pressure is increased, all membranes shown in **Figure 4** exhibit a decrease in permeance. However, the increase in the pressure differential across the membrane from increased feed pressure more than offsets the decrease in permeance, resulting in a net increase in flux for all membranes.

6. FUTURE OUTLOOK

It has been shown by process scale assessment that the current propane/propylene separation performance of ZIF-8 membranes meets the level required for industrial use (see detailed analysis presented in supporting information of Reference 12). First, it is important to note that distillation cannot be replaced by a single-stage ZIF-8 membrane of current performance, and although multistage membrane configurations like the ones disclosed by Colling et al. (169) may provide the ability to reach desirable purity and recovery, their competitiveness with distillation is not yet established. A feasible industrial use for ZIF-8 membranes is a hybrid membrane-distillation combination that can allow debottlenecking of existing distillation columns. A membrane with

a permeance of 100 GPU and separation factor of 50, when operated at 7 bar feed and 1 bar undiluted permeate, can accomplish a 35% increase in productivity (12). LIPS and GVD membranes have already demonstrated this level of performance, as shown in **Figure 4*d***. Even for a 50% reduction of the reboiler duty provided by heat integration (internal to the column or with the rest of the plant), such membranes can achieve ~25% savings in energy requirements compared to heat-integrated distillation. Although these potential energy savings are substantial, they represent less than 1% of the cost of polymer-grade propylene.

For this reason, energy savings may not be a sufficient incentive for industrial adaptation. Significant capital cost savings could enhance the likelihood of adapting this membrane technology. For a membrane with 100 GPU permeance and a separation factor of 50, operated at 7 bar feed and 1 bar permeate, the break-even capital cost can be achieved at an installed membrane cost of ~\$130/m^2 (12). Operation at 15 bar feed, assuming that the 100-GPU permeance is retained, allows a membrane cost of ~\$330/m^2. This cost limit and the need for large membrane areas (~5,000 m^2 to 10,000 m^2 to achieve production of 250,000 tonnes/year) point to scalable and low-cost production as a key for commercialization. Another attractive potential use of the propylene-selective membranes, the recovery of propylene that is lost in the purging process in polymerization plants, has also been analyzed (12, 170). This is a much smaller-scale and far less demanding application, which allows for installed membrane costs of up to ~\$1,000 to 10,000/m^2 and may serve as an entry point for ZIF-8 and other propylene-selective membranes.

ZIF-8 membranes can be fabricated using a wide range of conditions. This remarkable flexibility in choosing synthesis methods enables compatibility with various meso- and macroporous substrates and is an advantage toward scale-up and industrial development. Currently, none of the methods shown in **Figure 3** has been demonstrated to scale. We attempted to rank them with respect to potential for scalability in **Table 1**. In our view, the GVD membranes currently combine the required high-flux performance with potential for scalability, whereas other methods like DCTC and RTD, although meeting the scalability criterion, require significant improvements in flux. The LIPS method produces high-performance membranes, but its scalability relies on the scalability of ALD for thin-film formation in porous substrates (171), which is not yet established. Zhuang et al. (172) recently reported on an ALD reactor modeling study addressing this issue, revealing some of the potential challenges that have to be addressed at the ALD reactor level.

Compared to competing membranes like carbon molecular sieve (173) and polymeric membranes (174, 175), ZIF-8 is a material sensitive to moisture and other impurities like H_2S that may be encountered in industrial streams. H_2S exposure is expected to alter the separation performance of ZIF-8 membranes based on findings of H_2S surface reactions with ZIF-8 crystals (176). Because ZIF-8 is soluble in water (177), any contact with condensed water can be detrimental. Therefore, when applications are considered, one must carefully account for impurities and pretreatment methods for removing them before encountering the membrane. Other impurities that may be present in the membrane propane/propylene feeds depend on the membrane's placement in the separation sequence and include acetylene, methylacetylene, and propadiene, as well as C4 and C5 components (173). The performance of ZIF-8 membranes in the presence of such impurities should be evaluated and compared with that of other recently reported MOF membranes that are more stable, but also more difficult to fabricate (181).

7. CONCLUSION

ZIFs, and especially ZIF-8, are fundamentally fascinating materials owing to their structure and framework flexibility. The wide range of processing conditions that allow formation of thin films on various substrates have provided opportunities for innovative uses, with C3 separation being

the most prominent. Despite the progress achieved in meeting industrial flux and selectivity targets for use in hybrid membrane-distillation processes, scalable low-cost fabrication and stable performance in the presence of industrial feed-stream impurities have not been demonstrated.

DISCLOSURE STATEMENT

The authors are not aware of any affiliations, memberships, funding, or financial holdings that might be perceived as affecting the objectivity of this review.

ACKNOWLEDGMENTS

This material is based upon work supported by the US Department of Energy, Office of Science, Office of Basic Energy Sciences, Division of Chemical Sciences, Geosciences and Biosciences under award DE-SC0021212 and by a National Science Foundation award (CBET-1929596). Dr. Yurun Miao contributed to the text on framework flexibility.

LITERATURE CITED

1. Galizia M, Chi WS, Smith ZP, Merkel TC, Baker RW, Freeman BD. 2017. 50th anniversary perspective: polymers and mixed matrix membranes for gas and vapor separation: a review and prospective opportunities. *Macromolecules* 50:7809–43
2. Liu DF, Ma XL, Xi HX, Lin YS. 2014. Gas transport properties and propylene/propane separation characteristics of ZIF-8 membranes. *J. Membr. Sci.* 451:85–93
3. Koros WJ, Zhang C. 2017. Materials for next-generation molecularly selective synthetic membranes. *Nat. Mater.* 16:289–97
4. Koros WJ, Lively RP. 2012. Water and beyond: expanding the spectrum of large-scale energy efficient separation processes. *AIChE J.* 58:2624–33
5. Shekhah O, Chernikova V, Belmabkhout Y, Eddaoudi M. 2018. Metal–organic framework membranes: from fabrication to gas separation. *Crystals* 8:412
6. Pan Y, Li T, Lestari G, Lai Z. 2012. Effective separation of propylene/propane binary mixtures by ZIF-8 membranes. *J. Membr. Sci.* 390–91:93–98
7. Brown AJ, Brunelli NA, Eum K, Rashidi F, Johnson JR, et al. 2014. Interfacial microfluidic processing of metal-organic framework hollow fiber membranes. *Science* 345:72–75
8. Venna SR, Carreon MA. 2015. Metal organic framework membranes for carbon dioxide separation. *Chem. Eng. Sci.* 124:3–19
9. Kwon HT, Jeong H-K, Lee AS, An HS, Lee JS. 2015. Heteroepitaxially grown zeolitic imidazolate framework membranes with unprecedented propylene/propane separation performances. *J. Am. Chem. Soc.* 137:12304–11
10. Caro J. 2011. Are MOF membranes better in gas separation than those made of zeolites? *Curr. Opin. Chem. Eng.* 1:77–83
11. Gucuyener C, van den Bergh J, Gascon J, Kapteijn F. 2010. Ethane/ethene separation turned on its head: selective ethane adsorption on the metal-organic framework ZIF-7 through a gate-opening mechanism. *J. Am. Chem. Soc.* 132:17704–6
12. Ma XL, Kumar P, Mittal N, Khlyustova A, Daoutidis P, et al. 2018. Zeolitic imidazolate framework membranes made by ligand-induced permselectivation. *Science* 361:1008–11
13. Ma X, Liu D. 2019. Zeolitic imidazolate framework membranes for light olefin/paraffin separation. *Crystals* 9:14
14. Cacho-Bailo F, Caro G, Etxeberría-Benavides M, Karvan O, Téllez C, Coronas J. 2015. High selectivity ZIF-93 hollow fiber membranes for gas separation. *Chem. Commun.* 51:11283–85
15. Wang N, Liu Y, Qiao Z, Diestel L, Zhou J, et al. 2015. Polydopamine-based synthesis of a zeolite imidazolate framework ZIF-100 membrane with high H_2/CO_2 selectivity. *J. Mater. Chem. A* 3:4722–28
16. Huang K, Li Q, Liu G, Shen J, Guan K, Jin W. 2015. A ZIF-71 hollow fiber membrane fabricated by contra-diffusion. *ACS Appl. Mater. Interfaces* 7:16157–60

17. Li Y, Liang F, Bux H, Yang W, Caro J. 2010. Zeolitic imidazolate framework ZIF-7 based molecular sieve membrane for hydrogen separation. *J. Membr. Sci.* 354:48–54
18. Nian P, Liu H, Zhang X. 2019. Bottom-up fabrication of two-dimensional Co-based zeolitic imidazolate framework tubular membranes consisting of nanosheets by vapor phase transformation of Co-based gel for H_2/CO_2 separation. *J. Membr. Sci.* 573:200–9
19. Huang A, Chen Y, Wang N, Hu Z, Jiang J, Caro J. 2012. A highly permeable and selective zeolitic imidazolate framework ZIF-95 membrane for H_2/CO_2 separation. *Chem. Commun.* 48:10981–83
20. Li KH, Olson DH, Seidel J, Emge TJ, Gong HW, et al. 2009. Zeolitic imidazolate frameworks for kinetic separation of propane and propene. *J. Am. Chem. Soc.* 131:10368–69
21. Noh K, Lee J, Kim J. 2018. Compositions and structures of zeolitic imidazolate frameworks. *Isr. J. Chem.* 58:1075–88
22. Olujić Ž, Sun L, de Rijke A, Jansens PJ. 2006. Conceptual design of an internally heat integrated propylene-propane splitter. *Energy* 31:3083–96
23. Am. Chem. Counc. 2019. *Plastic Resins in the United States*. Washington, DC: Am. Chem. Counc.
24. Sholl DS, Lively RP. 2016. Seven chemical separations to change the world. *Nature* 532:435–37
25. Salgado-Gordon H-J, Valbuena-Moreno G. 2011. Technical and economic evaluation of the separation of light olefins (ethylene and propylene) by using π-complexation with silver salts. *CT&F* 4:73–87
26. Perry RH. 1997. *Perry's Chemical Engineers' Handbook*. New York: McGraw-Hill. 7th ed.
27. Motelica A, Bruinsma OSL, Kreiter R, den Exter M, Vente JF. 2012. Membrane retrofit option for paraffin/olefin separation—a technoeconomic evaluation. *Ind. Eng. Chem. Res.* 51:6977–86
28. Park KS, Ni Z, Cote AP, Choi JY, Huang RD, et al. 2006. Exceptional chemical and thermal stability of zeolitic imidazolate frameworks. *PNAS* 103:10186–91
29. Krokidas P, Castier M, Economou IG. 2017. Computational study of ZIF-8 and ZIF-67 performance for separation of gas mixtures. *J. Phys. Chem. C* 121:17999–8011
30. Peralta D, Chaplais G, Simon-Masseron A, Barthelet K, Chizallet C, et al. 2012. Comparison of the behavior of metal–organic frameworks and zeolites for hydrocarbon separations. *J. Am. Chem. Soc.* 134:8115–26
31. Bux H, Liang F, Li Y, Cravillon J, Wiebcke M, Caro J. 2009. Zeolitic imidazolate framework membrane with molecular sieving properties by microwave-assisted solvothermal synthesis. *J. Am. Chem. Soc.* 131:16000–1
32. Phan A, Doonan CJ, Uribe-Romo FJ, Knobler CB, O'Keeffe M, Yaghi OM. 2010. Synthesis, structure, and carbon dioxide capture properties of zeolitic imidazolate frameworks. *Acc. Chem. Res.* 43:58–67
33. Verploegh RJ, Nair S, Sholl DS. 2015. Temperature and loading-dependent diffusion of light hydrocarbons in ZIF-8 as predicted through fully flexible molecular simulations. *J. Am. Chem. Soc.* 137:15760–71
34. Coudert FX. 2017. Molecular mechanism of swing effect in zeolitic imidazolate framework ZIF-8: continuous deformation upon adsorption. *ChemPhysChem* 18:2732–38
35. Haldoupis E, Watanabe T, Nair S, Sholl DS. 2012. Quantifying large effects of framework flexibility on diffusion in MOFs: CH_4 and CO_2 in ZIF-8. *ChemPhysChem* 13:3449–52
36. Krokidas P, Castier M, Moncho S, Sredojevic DN, Brothers EN, et al. 2016. ZIF-67 framework: a promising new candidate for propylene/propane separation. Experimental data and molecular simulations. *J. Phys. Chem. C* 120:8116–24
37. Tan NY, Ruggiero MT, Orellana C, Tian T, Bond AD, et al. 2015. *Investigation of the terahertz vibrational modes of ZIF-8 and ZIF-90 with terahertz time-domain spectroscopy*. Presented at the 40th International Conference on Infrared, Millimeter and Terahertz Waves (Irmmw-Thz), Aug. 23–28, Hong Kong
38. Moggach SA, Bennett TD, Cheetham AK. 2009. The effect of pressure on ZIF-8: increasing pore size with pressure and the formation of a high-pressure phase at 1.47 GPa. *Angew. Chem. Int. Ed.* 48:7087–89
39. Fairen-Jimenez D, Moggach SA, Wharmby MT, Wright PA, Parsons S, Duren T. 2011. Opening the gate: framework flexibility in ZIF-8 explored by experiments and simulations. *J. Am. Chem. Soc.* 133:8900–2
40. Russell B, Villaroel J, Sapag K, Migone AD. 2014. O_2 adsorption on ZIF-8: temperature dependence of the gate-opening transition. *J. Phys. Chem. C* 118:28603–8
41. Zhang LL, Hu ZQ, Jiang JW. 2013. Sorption-induced structural transition of zeolitic imidazolate framework-8: a hybrid molecular simulation study. *J. Am. Chem. Soc.* 135:3722–28

42. Tanaka S, Fujita K, Miyake Y, Miyamoto M, Hasegawa Y, et al. 2015. Adsorption and diffusion phenomena in crystal size engineered ZIF-8 MOF. *J. Phys. Chem. C* 119:28430–39
43. Arami-Niya A, Birkett G, Zhu ZH, Rufford TE. 2017. Gate opening effect of zeolitic imidazolate framework ZIF-7 for adsorption of CH_4 and CO_2 from N_2. *J. Mater. Chem. A* 5:21389–99
44. Du Y, Mao KM, Wooler B, Sharma AK, Colmyer D, et al. 2017. Insights into the flexibility of ZIF-7 and its structural impact in alcohol adsorption. *J. Phys. Chem. C* 121:28090–95
45. Zheng B, Maurin G. 2019. Mechanical control of the kinetic propylene/propane separation by zeolitic imidazolate framework-8. *Angew. Chem. Int. Ed.* 58:13734–38
46. Zhang C, Gee JA, Sholl DS, Lively RP. 2014. Crystal-size-dependent structural transitions in nanoporous crystals: adsorption-induced transitions in ZIF-8. *J. Phys. Chem. C* 118:20727–33
47. Tanaka S, Sakamoto K, Inada H, Kawata M, Takasaki G, Imawaka K. 2018. Vapor-phase synthesis of ZIF-8 MOF thick film by conversion of ZnO nanorod array. *Langmuir* 34:7028–33
48. Tian T, Wharmby MT, Parra JB, Ania CO, Fairen-Jimenez D. 2016. Role of crystal size on swing-effect and adsorption induced structure transition of ZIF-8. *Dalton Trans.* 45:6893–900
49. Tiba A, Tivanski AV, MacGillivray LR. 2019. Size-dependent mechanical properties of a metal-organic framework: increase in flexibility of ZIF-8 by crystal downsizing. *Nano Lett.* 19:6140–43
50. Sheng LQ, Wang CQ, Yang F, Xiang L, Huang XJ, et al. 2017. Enhanced C_3H_6/C_3H_8 separation performance on MOF membranes through blocking defects and hindering framework flexibility by silicone rubber coating. *Chem. Commun.* 53:7760–63
51. Tan JC, Bennett TD, Cheetham AK. 2010. Chemical structure, network topology, and porosity effects on the mechanical properties of zeolitic imidazolate frameworks. *PNAS* 107:9938–43
52. Gao MZ, Wang J, Rong ZH, Shi Q, Dong JX. 2018. A combined experimental-computational investigation on water adsorption in various ZIFs with the SOD and RHO topologies. *RSC Adv.* 8:39627–34
53. Chaplais G, Fraux G, Paillaud J-L, Marichal C, Nouali H, et al. 2018. Impacts of the imidazolate linker substitution (CH_3, Cl, or Br) on the structural and adsorptive properties of ZIF-8. *The J. Phys. Chem. C* 122:26945–55
54. Morris W, Doonan CJ, Furukawa H, Banerjee R, Yaghi OM. 2008. Crystals as molecules: postsynthesis covalent functionalization of zeolitic imidazolate frameworks. *J. Am. Chem. Soc.* 130:12626–27
55. Eum K, Jayachandrababu KC, Rashidi F, Zhang K, Leisen J, et al. 2015. Highly tunable molecular sieving and adsorption properties of mixed-linker zeolitic imidazolate frameworks. *J. Am. Chem. Soc.* 137:4191–97
56. Zheng B, Wang LL, Du L, Huang K-W, Du H. 2016. ZIF-8 gate tuning via terminal group modification: a computational study. *Chem. Phys. Lett.* 658:270–75
57. Thompson JA, Blad CR, Brunelli NA, Lydon ME, Lively RP, et al. 2012. Hybrid zeolitic imidazolate frameworks: controlling framework porosity and functionality by mixed-linker synthesis. *Chem. Mater.* 24:1930–36
58. Hobday CL, Bennett TD, Fairen-Jimenez D, Graham AJ, Morrison CA, et al. 2018. Tuning the swing effect by chemical functionalization of zeolitic imidazolate frameworks. *J. Am. Chem. Soc.* 140:382–87
59. Liu D, Wu Y, Xia Q, Li Z, Xi H. 2013. Experimental and molecular simulation studies of CO_2 adsorption on zeolitic imidazolate frameworks: ZIF-8 and amine-modified ZIF-8. *Adsorption* 19:25–37
60. Schejn A, Aboulaich A, Balan L, Falk V, Lalevee J, et al. 2015. Cu^{2+}-doped zeolitic imidazolate frameworks (ZIF-8): efficient and stable catalysts for cycloadditions and condensation reactions. *Catal. Sci. Technol.* 5:1829–39
61. Li R, Ren X, Feng X, Li X, Hu C, Wang B. 2014. A highly stable metal- and nitrogen-doped nanocomposite derived from Zn/Ni-ZIF-8 capable of CO_2 capture and separation. *Chem. Commun.* 50:6894–97
62. Krokidas P, Moncho S, Brothers EN, Castier M, Economou IG. 2018. Tailoring the gas separation efficiency of metal organic framework ZIF-8 through metal substitution: a computational study. *Phys. Chem. Chem. Phys.* 20:4879–92
63. Tian YQ, Yao SY, Gu D, Cui KH, Guo DW, et al. 2010. Cadmium imidazolate frameworks with polymorphism, high thermal stability, and a large surface area. *Chemistry* 16:1137–41
64. Banerjee R, Phan A, Wang B, Knobler C, Furukawa H, et al. 2008. High-throughput synthesis of zeolitic imidazolate frameworks and application to CO_2 capture. *Science* 319:939–43

65. Qian JF, Sun FA, Qin LZ. 2012. Hydrothermal synthesis of zeolitic imidazolate framework-67 (ZIF-67) nanocrystals. *Mater. Lett.* 82:220–23
66. McGuirk CM, Runcevski T, Oktawiec J, Turkiewicz A, Taylor MK, Long JR. 2018. Influence of metal substitution on the pressure-induced phase change in flexible zeolitic imidazolate frameworks. *J. Am. Chem. Soc.* 140:15924–33
67. Fei HH, Cahill JF, Prather KA, Cohen SM. 2013. Tandem postsynthetic metal ion and ligand exchange in zeolitic imidazolate frameworks. *Inorg. Chem.* 52:4011–16
68. Thompson JA, Brunelli NA, Lively RP, Johnson JR, Jones CW, Nair S. 2013. Tunable CO_2 adsorbents by mixed-linker synthesis and postsynthetic modification of zeolitic imidazolate frameworks. *J. Phys. Chem. C* 117:8198–207
69. Karagiaridi O, Lalonde MB, Bury W, Sarjeant AA, Farha OK, Hupp JT. 2012. Opening ZIF-8: a catalytically active zeolitic imidazolate framework of sodalite topology with unsubstituted linkers. *J. Am. Chem. Soc.* 134:18790–96
70. Hillman F, Jeong H-K. 2019. Linker-doped zeolitic imidazolate frameworks (ZIFs) and their ultrathin membranes for tunable gas separations. *ACS Appl. Mater. Interfaces* 11:18377–85
71. Karagiaridi O, Bury W, Sarjeant AA, Stern CL, Farha OK, Hupp JT. 2012. Synthesis and characterization of isostructural cadmium zeolitic imidazolate frameworks via solvent-assisted linker exchange. *Chem. Sci.* 3:3256–60
72. Jayachandrababu KC, Sholl DS, Nair S. 2017. Structural and mechanistic differences in mixed-linker zeolitic imidazolate framework synthesis by solvent assisted linker exchange and *de novo* routes. *J. Am. Chem. Soc.* 139:5906–15
73. Ban YJ, Peng Y, Zhang YL, Jin H, Jiao WM, et al. 2016. Dual-ligand zeolitic imidazolate framework crystals and oriented films derived from metastable mono-ligand ZIF-108. *Microporous Mesoporous Mater.* 219:190–98
74. Sánchez-Laínez J, Veiga A, Zornoza B, Balestra SRG, Hamad S, et al. 2017. Tuning the separation properties of zeolitic imidazolate framework core-shell structures *via* post-synthetic modification. *J. Mater. Chem. A* 5:25601–08
75. Hou QQ, Wu Y, Zhou S, Wei YY, Caro J, Wang HH. 2019. Ultra-tuning of the aperture size in stiffened ZIF-8_Cm frameworks with mixed-linker strategy for enhanced CO_2/CH_4 separation. *Angew. Chem. Int. Ed.* 58:327–31
76. Verploegh RJ, Wu Y, Sholl DS. 2017. Lattice-gas modeling of adsorbate diffusion in mixed-linker zeolitic imidazolate frameworks: effect of local imidazolate ordering. *Langmuir* 33:6481–91
77. Venna SR, Jasinski JB, Carreon MA. 2010. Structural evolution of zeolitic imidazolate framework-8. *J. Am. Chem. Soc.* 132:18030–33
78. Lee YR, Jang MS, Cho BY, Kwon HJ, Kim S, Ahn WS. 2015. ZIF-8: a comparison of synthesis methods. *Chem. Eng. J.* 271:276–80
79. Anumah A, Louis H, Saud-uz-Zafar, Hamzat AT, Amusan OO, et al. 2019. Metal-organic frameworks (MOFs): recent advances in synthetic methodologies and some applications. *Chem. Methodol.* 3:283–305
80. Lee YR, Kim J, Ahn WS. 2013. Synthesis of metal-organic frameworks: a mini review. *Korean J. Chem. Eng.* 30:1667–80
81. Zhang HF, Zhao M, Lin YS. 2019. Stability of ZIF-8 in water under ambient conditions. *Microporous Mesoporous Mater.* 279:201–10
82. Jian MP, Liu B, Liu RP, Qu JH, Wang HT, Zhang XW. 2015. Water-based synthesis of zeolitic imidazolate framework-8 with high morphology level at room temperature. *RSC Adv.* 5:48433–41
83. Cravillon J, Nayuk R, Springer S, Feldhoff A, Huber K, Wiebcke M. 2011. Controlling zeolitic imidazolate framework nano- and microcrystal formation: insight into crystal growth by time-resolved in situ static light scattering. *Chem. Mater.* 23:2130–41
84. Ban YJ, Li YS, Liu XL, Peng Y, Yang WS. 2013. Solvothermal synthesis of mixed-ligand metal-organic framework ZIF-78 with controllable size and morphology. *Microporous Mesoporous Mater.* 173:29–36
85. Khaleque A, Alam MM, Hoque M, Mondal S, Haider JB, et al. 2020. Zeolite synthesis from low-cost materials and environmental applications: a review. *Environ. Adv.* 2:10019
86. Huang XC, Lin YY, Zhang JP, Chen XM. 2006. Ligand-directed strategy for zeolite-type metal-organic frameworks: zinc(II) imidazolates with unusual zeolitic topologies. *Angew. Chem. Int. Ed.* 45:1557–59

87. Bustamante EL, Fernández JL, Zamaro JM. 2014. Influence of the solvent in the synthesis of zeolitic imidazolate framework-8 (ZIF-8) nanocrystals at room temperature. *J. Colloid Interface Sci.* 424:37–43
88. Cravillon J, Schröder CA, Nayuk R, Gummel J, Huber K, Wiebcke M. 2011. Fast nucleation and growth of ZIF-8 nanocrystals monitored by time-resolved in situ small-angle and wide-angle X-ray scattering. *Angew. Chem. Int. Ed.* 50:8067–71
89. Ozturk Z, Filez M, Weckhuysen BM. 2017. Decoding nucleation and growth of zeolitic imidazolate framework thin films with atomic force microscopy and vibrational spectroscopy. *Chemistry* 23:10915–24
90. Chen BL, Yang ZX, Zhu YQ, Xia YD. 2014. Zeolitic imidazolate framework materials: recent progress in synthesis and applications. *J. Mater. Chem. A* 2:16811–31
91. Pan YC, Liu YY, Zeng GF, Zhao L, Lai ZP. 2011. Rapid synthesis of zeolitic imidazolate framework-8 (ZIF-8) nanocrystals in an aqueous system. *Chem. Commun.* 47:2071–73
92. Tanaka S, Kida K, Okita M, Ito Y, Miyake Y. 2012. Size-controlled synthesis of zeolitic imidazolate framework-8 (ZIF-8) crystals in an aqueous system at room temperature. *Chem. Lett.* 41:1337–39
93. Kida K, Okita M, Fujita K, Tanaka S, Miyake Y. 2013. Formation of high crystalline ZIF-8 in an aqueous solution. *CrystEngComm* 15:1794–801
94. Malekmohammadi M, Fatemi S, Razavian M, Nouralishahi A. 2019. A comparative study on ZIF-8 synthesis in aqueous and methanolic solutions: effect of temperature and ligand content. *Solid State Sci.* 91:108–12
95. Bao QL, Lou YB, Xing TT, Chen JX. 2013. Rapid synthesis of zeolitic imidazolate framework-8 (ZIF-8) in aqueous solution via microwave irradiation. *Inorg. Chem. Commun.* 37:170–73
96. Fan XX, Wang W, Li W, Zhou JW, Wang B, et al. 2014. Highly porous ZIF-8 nanocrystals prepared by a surfactant mediated method in aqueous solution with enhanced adsorption kinetics. *ACS Appl. Mater. Interfaces* 6:14994–99
97. Gross AF, Sherman E, Vajo JJ. 2012. Aqueous room temperature synthesis of cobalt and zinc sodalite zeolitic imidizolate frameworks. *Dalton Trans.* 41:5458–60
98. He M, Yao JF, Liu Q, Wang K, Chen FY, Wang HT. 2014. Facile synthesis of zeolitic imidazolate framework-8 from a concentrated aqueous solution. *Microporous Mesoporous Mater.* 184:55–60
99. Nordin NAHM, Ismail AF, Mustafa A, Goh PS, Rana D, Matsuura T. 2014. Aqueous room temperature synthesis of zeolitic imidazole framework 8 (ZIF-8) with various concentrations of triethylamine. *RSC Adv.* 4:33292–300
100. Wu RF, Fan T, Chen JY, Li YW. 2019. Synthetic factors affecting the scalable production of zeolitic imidazolate frameworks. *ACS Sustain. Chem. Eng.* 7:3632–46
101. Shi Q, Chen ZF, Song ZW, Li JP, Dong JX. 2011. Synthesis of ZIF-8 and ZIF-67 by steam-assisted conversion and an investigation of their tribological behaviors. *Angew. Chem. Int. Ed.* 50:672–75
102. Ahmed I, Jeon J, Khan NA, Jhung SH. 2012. Synthesis of a metal-organic framework, iron-benezenetricarboxylate, from dry gels in the absence of acid and salt. *Cryst. Growth Des.* 12:5878–81
103. Chen Y, Yang CY, Wang XQ, Yang JF, Li JP. 2017. Vapor phase solvents loaded in zeolite as the sustainable medium for the preparation of Cu-BTC and ZIF-8. *Chem. Eng. J.* 313:179–86
104. Stassen I, Styles M, Grenci G, Van Gorp H, Vanderlinden W, et al. 2016. Chemical vapour deposition of zeolitic imidazolate framework thin films. *Nat. Mater.* 15:304–10
105. Cruz AJ, Stassen I, Krishtab M, Marcoen K, Stassin T, et al. 2019. Integrated cleanroom process for the vapor-phase deposition of large-area zeolitic imidazolate framework thin films. *Chem. Mater.* 31:9462–71
106. Huang JK, Saito N, Cai YC, Wan Y, Cheng CC, et al. 2020. Steam-assisted chemical vapor deposition of zeolitic imidazolate framework. *ACS Mater. Lett.* 2:485–91
107. López-Cabrelles J, Romero J, Abellán G, Giménez-Marqués M, Palomino M, et al. 2019. Solvent-free synthesis of ZIFs: a route toward the elusive Fe(II) analogue of ZIF-8. *J. Am. Chem. Soc.* 141:7173–80
108. Marreiros J, Van Dommelen L, Fleury G, de Oliveira-Silva R, Stassin T, et al. 2019. Vapor-phase linker exchange of the metal-organic framework ZIF-8: a solvent-free approach to post-synthetic modification. *Angew. Chem. Int. Ed.* 58:18471–75
109. Eum K, Hayashi M, De Mello MD, Xue F, Kwon HT, Tsapatsis M. 2019. ZIF-8 membrane separation performance tuning by vapor phase ligand treatment. *Angew. Chem. Int. Ed.* 58:16390–94

110. Wu WF, Su JY, Jia MM, Li ZJ, Liu GQ, Li WB. 2020. Vapor-phase linker exchange of metal-organic frameworks. *Sci. Adv.* 6:eaax7270
111. Qiu S, Xue M, Zhu G. 2014. Metal-organic framework membranes: from synthesis to separation application. *Chem. Soc. Rev.* 43:6116–40
112. Qian Q, Asinger PA, Lee MJ, Han G, Mizrahi Rodriguez K, et al. 2020. MOF-based membranes for gas separations. *Chem. Rev.* 120:8161–266
113. Shah M, McCarthy MC, Sachdeva S, Lee AK, Jeong H-K. 2012. Current status of metal–organic framework membranes for gas separations: promises and challenges. *Ind. Eng. Chem. Res.* 51:2179–99
114. Abdul Hamid MR, Shean Yaw TC, Mohd Tohir MZ, Ghani WAWAK, Sutrisna PD, Jeong H-K. 2021. Zeolitic imidazolate framework membranes for gas separations: current state-of-the-art, challenges, and opportunities. *J. Ind. Eng. Chem.* 98:17–41
115. Lee MJ, Kwon HT, Jeong H-K. 2018. High-flux zeolitic imidazolate framework membranes for propylene/propane separation by postsynthetic linker exchange. *Angew. Chem. Int. Ed.* 57:156–61
116. Hayashi M, Lee DT, de Mello MD, Boscoboinik JA, Tsapatsis M. 2021. ZIF-8 membrane permselectivity modification by manganese(II) acetylacetonate vapor treatment. *Angew. Chem. Int. Ed.* 60:9316–20
117. Miao Y, Lee DT, Dorneles de Mello M, Abdel-Rahman MK, Corkery P, et al. 2021. Electron beam induced modification of ZIF-8 membrane permeation properties. *Chem. Commun.* 57:5250–53
118. Gitis V, Rothenberg G. 2016. The basics. In *Ceramic Membranes: New Opportunities and Practical Applications*, ed. V Gitis, G Rothenberg, pp. 1–90. Weinheim, Ger.: Wiley-VCH Verlag
119. James JB, Lin YS. 2017. Thermal stability of ZIF-8 membranes for gas separations. *J. Membr. Sci.* 532:9–19
120. Drioli E, Giorno L. 2010. *Comprehensive Membrane Science and Engineering*. Amsterdam/Boston: Elsevier/Academic
121. Li Y, Yang W. 2008. Microwave synthesis of zeolite membranes: a review. *J. Membr. Sci.* 316:3–17
122. Neelakanda P, Barankova E, Peinemann K-V. 2016. Polymer supported ZIF-8 membranes by conversion of sputtered zinc oxide layers. *Microporous Mesoporous Mater.* 220:215–19
123. Huang A, Bux H, Steinbach F, Caro J. 2010. Molecular-sieve membrane with hydrogen permselectivity: ZIF-22 in LTA topology prepared with 3-aminopropyltriethoxysilane as covalent linker. *Angew. Chem. Int. Ed.* 49:4958–61
124. Huang A, Dou W, Caro J. 2010. Steam-stable zeolitic imidazolate framework ZIF-90 membrane with hydrogen selectivity through covalent functionalization. *J. Am. Chem. Soc.* 132:15562–64
125. Peterson GW, Lee DT, Barton HF, Epps TH III, Parsons GN. 2021. Fibre-based composites from the integration of metal–organic frameworks and polymers. *Nat. Rev. Mater.* 6:605–21
126. Kwon HT, Jeong H-K. 2013. Highly propylene-selective supported zeolite-imidazolate framework (ZIF-8) membranes synthesized by rapid microwave-assisted seeding and secondary growth. *Chem. Commun.* 49:3854–56
127. Li YS, Liang FY, Bux H, Feldhoff A, Yang WS, Caro J. 2010. Molecular sieve membrane: supported metal-organic framework with high hydrogen selectivity. *Angew. Chem. Int. Ed.* 49:548–51
128. Shekhah O, Swaidan R, Belmabkhout Y, du Plessis M, Jacobs T, et al. 2014. The liquid phase epitaxy approach for the successful construction of ultra-thin and defect-free ZIF-8 membranes: pure and mixed gas transport study. *Chem. Commun.* 50:2089–92
129. Kwon HT, Jeong H-K. 2013. *In situ* synthesis of thin zeolitic-imidazolate framework ZIF-8 membranes exhibiting exceptionally high propylene/propane separation. *J. Am. Chem. Soc.* 135:10763–68
130. Xie Z, Yang J, Wang J, Bai J, Yin H, et al. 2012. Deposition of chemically modified α-Al_2O_3 particles for high performance ZIF-8 membrane on a macroporous tube. *Chem. Commun.* 48:5977–79
131. Shah MN, Gonzalez MA, McCarthy MC, Jeong H-K. 2013. An unconventional rapid synthesis of high performance metal-organic framework membranes. *Langmuir* 29:7896–902
132. Ma Q, Mo K, Gao S, Xie Y, Wang J, et al. 2020. Ultrafast semi-solid processing of highly durable ZIF-8 membranes for propylene/propane separation. *Angew. Chem. Int. Ed.* 59:21909–14
133. Ameloot R, Gobechiya E, Uji-i H, Martens JA, Hofkens J, et al. 2010. Direct patterning of oriented metal–organic framework crystals via control over crystallization kinetics in clear precursor solutions. *Adv. Mater.* 22:2685–88

134. Hao J, Babu DJ, Liu Q, Chi H-Y, Lu C, et al. 2020. Synthesis of high-performance polycrystalline metal–organic framework membranes at room temperature in a few minutes. *J. Mater. Chem. A* 8:7633–40
135. He G, Dakhchoune M, Zhao J, Huang S, Agrawal KV. 2018. Electrophoretic nuclei assembly for crystallization of high-performance membranes on unmodified supports. *Adv. Funct. Mater.* 28:1707427
136. Zhou S, Wei YY, Li LB, Duan YF, Hou QQ, et al. 2018. Paralyzed membrane: current-driven synthesis of a metal-organic framework with sharpened propene/propane separation. *Sci. Adv.* 4:eaau1393
137. Wei R, Chi HY, Li X, Lu D, Wan Y, et al. 2019. Aqueously cathodic deposition of ZIF-8 membranes for superior propylene/propane separation. *Adv. Funct. Mater.* 30:1907089
138. Hou Q, Zhou S, Wei Y, Caro J, Wang H. 2020. Balancing the grain boundary structure and the framework flexibility through bimetallic metal-organic framework (MOF) membranes for gas separation. *J. Am. Chem. Soc.* 142:9582–86
139. Zhang YY, Feng X, Yuan S, Zhou JW, Wang B. 2016. Challenges and recent advances in MOF-polymer composite membranes for gas separation. *Inorg. Chem. Front.* 3:896–909
140. Baker RW. 2004. Membranes and modules. In *Membrane Technology and Applications*, ed. RW Baker, pp. 89–160. Hoboken, NJ: John Wiley & Sons. 2nd ed.
141. Lau CH, Low BT, Shao L, Chung T-S. 2010. A vapor-phase surface modification method to enhance different types of hollow fiber membranes for industrial scale hydrogen separation. *Int. J. Hydrogen Energy* 35:8970–82
142. Yao J, Dong D, Li D, He L, Xu G, Wang H. 2011. Contra-diffusion synthesis of ZIF-8 films on a polymer substrate. *Chem. Commun.* 47:2559–61
143. Cacho-Bailo F, Seoane B, Téllez C, Coronas J. 2014. ZIF-8 continuous membrane on porous polysulfone for hydrogen separation. *J. Membr. Sci.* 464:119–26
144. Li W, Yang Z, Zhang G, Fan Z, Meng Q, et al. 2014. Stiff metal–organic framework–polyacrylonitrile hollow fiber composite membranes with high gas permeability. *J. Mater. Chem. A* 2:2110–18
145. Li W, Meng Q, Zhang C, Zhang G. 2015. Metal-organic framework/PVDF composite membranes with high H_2 permselectivity synthesized by ammoniation. *Chemistry* 21:7224–30
146. Shamsaei E, Low ZX, Lin X, Mayahi A, Liu H, et al. 2015. Rapid synthesis of ultrathin, defect-free ZIF-8 membranes via chemical vapour modification of a polymeric support. *Chem. Commun.* 51:11474–77
147. Shamsaei E, Lin X, Low ZX, Abbasi Z, Hu Y, et al. 2016. Aqueous phase synthesis of ZIF-8 membrane with controllable location on an asymmetrically porous polymer substrate. *ACS Appl. Mater. Interfaces* 8:6236–44
148. Barankova E, Tan X, Villalobos LF, Litwiller E, Peinemann KV. 2017. A metal chelating porous polymeric support: the missing link for a defect-free metal-organic framework composite membrane. *Angew. Chem. Int. Ed.* 56:2965–68
149. Su P, Li W, Zhang C, Meng Q, Shen C, Zhang G. 2015. Metal based gels as versatile precursors to synthesize stiff and integrated MOF/polymer composite membranes. *J. Mater. Chem. A* 3:20345–51
150. Li W, Su P, Li Z, Xu Z, Wang F, et al. 2017. Ultrathin metal-organic framework membrane production by gel-vapour deposition. *Nat. Commun.* 8:406
151. Tanaka S, Okubo K, Kida K, Sugita M, Takewaki T. 2017. Grain size control of ZIF-8 membranes by seeding-free aqueous synthesis and their performances in propylene/propane separation. *J. Membr. Sci.* 544:306–11
152. Pan YC, Liu W, Zhao YJ, Wang CQ, Lai ZP. 2015. Improved ZIF-8 membrane: effect of activation procedure and determination of diffusivities of light hydrocarbons. *J. Membr. Sci.* 493:88–96
153. Kwon HT, Jeong H-K. 2015. Improving propylene/propane separation performance of zeolitic-imidazolate framework ZIF-8 membranes. *Chem. Eng. Sci.* 124:20–26
154. Hara N, Yoshimune M, Negishi H, Haraya K, Hara S, Yamaguchi T. 2014. Thickness reduction of the zeolitic imidazolate framework-8 membrane by controlling the reaction rate during the membrane preparation. *J. Chem. Eng. Japan* 47:770–76
155. Hara N, Yoshimune M, Negishi H, Haraya K, Hara S, Yamaguchi T. 2014. Diffusive separation of propylene/propane with ZIF-8 membranes. *J. Membr. Sci.* 450:215–23
156. Hara N, Yoshimune M, Negishi H, Haraya K, Hara S, Yamaguchi T. 2015. Effect of temperature on synthesis of ZIF-8 membranes for propylene/propane separation by counter diffusion method. *J. Japan Pet. Inst.* 58:237–44

157. Eum K, Ma C, Rownaghi A, Jones CW, Nair S. 2016. ZIF-8 membranes via interfacial microfluidic processing in polymeric hollow fibers: efficient propylene separation at elevated pressures. *ACS Appl. Mater. Interfaces* 8:25337–42
158. Li JF, Lian HQ, Wei KF, Song EY, Pan YC, Xing WH. 2020. Synthesis of tubular ZIF-8 membranes for propylene/propane separation under high-pressure. *J. Membr. Sci.* 595:117503
159. Glob. Ind. Anal. 2021. *Propylene: global market trajectory & analytics*. Rep. 4845833, Glob. Ind. Anal. **https://www.researchandmarkets.com/reports/4845833/propylene-global-market-trajectory-and-analytics**
160. Silva FAD, Rodrigues AE. 2001. Propylene/propane separation by vacuum swing adsorption 13X zeolite. *AIChE J.* 47:341–57
161. Zhang C, Lively RP, Zhang K, Johnson JR, Karvan O, Koros WJ. 2012. Unexpected molecular sieving properties of zeolitic imidazolate framework-8. *J. Phys. Chem. Lett.* 3:2130–34
162. Qiao ZH, Liang YY, Zhang ZQ, Mei DH, Wang Z, et al. 2020. Ultrathin low-crystallinity MOF membranes fabricated by interface layer polarization induction. *Adv. Mater.* 32:2002165
163. Huang K, Wang B, Chi YS, Li K. 2018. High propylene selective metal-organic framework membranes prepared in confined spaces via convective circulation synthesis. *Adv. Mater. Interfaces* 5:1800287
164. Lee MJ, Kwon HT, Jeong H-K. 2017. Defect-dependent stability of highly propylene-selective zeolitic-imidazolate framework ZIF-8 membranes. *J. Membr. Sci.* 529:105–13
165. Lee MJ, Hamid MRA, Lee J, Kim JS, Lee YM, Jeong H-K. 2018. Ultrathin zeolitic-imidazolate framework ZIF-8 membranes on polymeric hollow fibers for propylene/propane separation. *J. Membr. Sci.* 559:28–34
166. Rashidi F, Leisen J, Kim SJ, Rownaghi AA, Jones CW, Nair S. 2019. All-nanoporous hybrid membranes: redefining upper limits on molecular separation properties. *Angew. Chem. Int. Ed.* 58:236–39
167. Jogwar SS, Daoutidis P. 2009. Dynamics and control of vapor recompression distillation. *J. Process Control* 19:1737–50
168. Yu J, Pan YC, Wang CQ, Lai ZP. 2016. ZIF-8 membranes with improved reproducibility fabricated from sputter-coated ZnO/alumina supports. *Chem. Eng. Sci.* 141:119–24
169. Colling CW, Huff GA Jr., Bartels JV. 2004. *Processes using solid perm-selective membranes in multiple groups for simultaneous recovery of specified products from a fluid mixture*. US Patent No. 2004/0004040 A1
170. Castoldi MT, Pinto JC, Melo PA. 2007. Modeling of the separation of propene/propane mixtures by permeation through membranes in a polymerization system. *Ind. Eng. Chem. Res.* 46:1259–69
171. Drobek M, Bechelany M, Vallicari C, Abou Chaaya A, Charmette C, et al. 2015. An innovative approach for the preparation of confined ZIF-8 membranes by conversion of ZnO ALD layers. *J. Membr. Sci.* 475:39–46
172. Zhuang L, Corkery P, Lee DT, Lee S, Kooshkbaghi M, et al. 2021. Numerical simulation of atomic layer deposition for thin deposit formation in a mesoporous substrate. *AIChE J.* 67:e17305
173. Xu L, Rungta M, Brayden MK, Martinez MV, Stears BA, et al. 2012. Olefins-selective asymmetric carbon molecular sieve hollow fiber membranes for hybrid membrane-distillation processes for olefin/paraffin separations. *J. Membr. Sci.* 423–24:314–23
174. Feiring AE, Lazzeri J, Majumdar S, Shangguan N. 2018. *Membrane separation of olefin and paraffin mixtures*. US Patent No. 10,029,248
175. Staudt-Bickel C, Koros WJ. 2000. Olefin/paraffin gas separations with 6FDA-based polyimide membranes. *J. Membr. Sci.* 170:205–14
176. Dutta A, Tymińska N, Zhu G, Collins J, Lively RP, et al. 2018. Influence of hydrogen sulfide exposure on the transport and structural properties of the metal–organic framework ZIF-8. *J. Phys. Chem. C* 122:7278–87
177. Zhang HF, James J, Zhao M, Yao Y, Zhang YS, et al. 2017. Improving hydrostability of ZIF-8 membranes via surface ligand exchange. *J. Membr. Sci.* 532:1–8
178. Song EY, Wei KF, Lian HQ, Hua JX, Tao HX, et al. 2021. Improved propylene/propane separation performance under high temperature and pressures on in-situ ligand-doped ZIF-8 membranes. *J. Membr. Sci.* 617:118655

179. Abdul Hamid MR, Kim S, Kim JS, Lee YM, Jeong H-K. 2019. *In situ* formation of zeolitic-imidazolate framework thin films and composites using modified polymer substrates. *J. Mater. Chem. A* 7:9680–89
180. Wang YH, Fin H, Ma Q, Mo K, Mao HZ, et al. 2020. A MOF glass membrane for gas separation. *Angew. Chem. Int. Ed.* 59:4365–69
181. Zhou S, Shekhah O, Jia J, Czaban-Jóźwiak J, Bhatt PM, et al. 2021. Electrochemical synthesis of continuous metal-organic framework membranes for separation of hydrocarbons. *Nat. Energy* 6:882–91

Annual Review of Chemical and Biomolecular Engineering

Volume 13, 2022

Contents

Errata

An online log of corrections to *Annual Review of Chemical and Biomolecular Engineering* articles may be found at http://www.annualreviews.org/errata/chembioeng